

# **Determination of Clinical Efficacy of Ultrasound Stimulation on Piezoelectric Composites for Power Generation Applications**

By  
Morghan Alters

Submitted to the graduate degree program in Bioengineering and the Graduate Faculty of the University of Kansas in partial fulfillment of the requirements for the degree of Master of Science.

---

Chairperson

Dr. Elizabeth Friis

---

Dr. Linda D'Silva

---

Dr. Carl Luchies

Date Defended: December 11, 2019

The Thesis Committee for Morghan Alters  
certifies that this is the approved version of the following thesis:

Determination of Clinical Efficacy of Ultrasound Stimulation on Piezoelectric  
Composites for Power Generation Applications

---

Chairperson

Dr. Elizabeth Friis

Date Approved: December 11, 2019

## Abstract

Each year in the United States there are over one million fractures that occur [1]. When a bone breaks, regardless of the severity, it is referred to as a fracture. Individuals suffering from a fracture typically undergo some form of clinical intervention ranging from a splint to orthopedic surgery to increase the body's natural ability to fuse the bone. This does not always occur, and some fractures never fuse resulting in a non-union. Bone stimulating adjunct therapies are available, to aid in bone healing, but often require patient compliance or battery packs, but these therapies have restrictions too such as the limited lifespan of batteries. Self-powered generators comprised of piezoelectric composite materials have shown promising results in bone stimulation applications under physiological loading conditions. To increase the effectiveness of these materials in clinical applications the use of ultrasound loading was investigated for use when physiological loading is not possible. Twelve piezoelectric composite specimens (n=6 for both 0.0 mm and 0.8 mm CLACS groups) were manufactured using three stacked, lead zirconate titanate (PZT) discs, wired with the intent to be connected in parallel, encapsulated with medical grade epoxy. The effect of ultrasound intensity (0.1, 0.5, and 1.0 W/cm<sup>2</sup>), compliant layer thickness (0.0 mm and 0.8 mm), and ultrasound application angle (0°, 45°, and 90°) on power generation was investigated for all specimens. An increase in ultrasound intensity resulted in an increase in power production for all specimens. At an application angle of 0° the 0.8 mm CLACS group produced more power than the 0.0 mm group, but a reversed trend was observed at angles of 45° and 90°. Lastly, when compared to 0°, the power output of both specimen groups decreased significantly in the 45° and 90° conditions at all intensities. This study demonstrates that ultrasound is a viable option for stimulating PZT composites intended for power generating applications where physiological loading is not applicable.

## Acknowledgements

### **Dr. Elizabeth Friis**

I would like to thank Dr. Friis for giving me the opportunity to work in her lab. Over the course of my graduate career I have not only accumulated knowledge necessary for this research project, but I have also gained knowledge in areas that will help me in my professional career. As Dr. Friis would call it “adding tools to your tool kit”. I am grateful for her all of her input, guidance, and support she has offered every step of the way.

### **Dr. Linda D’Silva**

I would like to thank Dr. D’Silva for her willingness to help, cheerfulness, and for lending me the ultrasound unit necessary for this research project.

### **Dr. Carl Luchies**

I would like to thank Dr. Luchies for his willingness to help and answer questions, as well as his desire for students to succeed. I learned a lot from Dr. Luchies in the classes he taught and only wished I had taken more.

### **Dr. Terence McIff**

During this research project our ultrasound unit was unusable and Dr. McIff assisted me in obtaining a new one. Therefore, I would like to thank Dr. McIff for taking the time to tour the University of Kansas Medical Center and facilitate the introductions necessary to obtain the required equipment.

### **My lab mates at the University of Kansas**

I would like to thank my lab mates Chris Bowen, Kyle Coates, Craig Cunningham, Ryan Downing, Tori Drapel, Josh Koski, Ember Krech, Zach Pessia, and Chris Tacca for always being there to lend an ear, have a good laugh, celebrate labs-giving, Christmas mug exchanges, and happy hour birthday celebrations with giant Jenga. Aside from all these I am thankful for you all always being there to share your

knowledge, brain storm, and lift each other spirits. You have made my graduate career much more enjoyable.

### **My Family**

I would like to thank my parents and siblings for always supporting me. Although you are miles away you were always a phone call away. My research and school work may have sounded like a second language to you, but you always listened and believed in me. Thank you for always being in my corner cheering me on.

### **Logan Sidener**

I would like to thank Logan Sidener for being one of my biggest fans. Thank you for always listening to me vent about how frustrating my research was being and reminding me that was research, for celebrating every success along the way and reminding me that even the smallest successes are still a success, and for always believing in me.

This work was supported by KU Go **Grant (insert Grant Number here).**

## Table of Contents

Abstract.....	iii
Acknowledgements .....	iv
List of Figures.....	viii
List of Tables .....	viii
List of Equations.....	viii
Chapter 1: Introduction.....	1
1.1 Background and Motivation .....	1
1.2 Specific Aims .....	2
Chapter 2: Background and Literature Review .....	3
2.1 Bone Remodeling and Healing.....	3
2.1.1 Wolff's Law .....	3
2.1.2 The Wnt Pathway.....	4
2.1.3 Compromised Bone .....	5
2.1.4 Bone Stimulators.....	5
2.1.5 Electrical Stimulation.....	7
2.2 Piezoelectricity .....	8
2.2.1 Piezoelectric Effect .....	8
2.2.2 Synthetic Materials .....	9
2.2.3 Piezoelectric Constants .....	10
2.2.4 Applications .....	11
2.2.5 Stacked Composites .....	11
2.2.6 Piezoelectric Materials in Bone Stimulation.....	13
2.3 Ultrasound .....	14
2.3.1 Ultrasound Parameters .....	15
2.3.2 Diagnostic versus Therapeutic Ultrasound .....	16
2.4 Tissue Mimicking Phantoms .....	18
2.5 References .....	20
Chapter 3: Journal of Medical Devices Research Paper (In Progress) .....	23
3.1 Abstract .....	24
3.2 Introduction .....	24
3.3 Methods.....	27
3.3.1 Composite Material Identification .....	27
3.3.2 Specimen Fabrication.....	27
3.3.3 Ultrasound Testing.....	29
3.3.4 Data and Statistical Analysis.....	30

3.4 Results .....	30
3.4.1 Complete Stacks.....	31
3.4.2 Individual Disc Contribution .....	34
3.5 Discussion .....	34
3.6 Conclusion.....	37
3.7 Acknowledgements .....	38
3.8 Funding Data .....	38
3.9 Nomenclature .....	38
3.10 References .....	38
Chapter 4: Conclusions and Future Work.....	40
4.1 Conclusions .....	40
4.2 Limitations .....	40
4.3 Future Work .....	41
Appendix A: Supplementary Figures .....	42
Appendix B: Detailed Methods .....	46
Fabrication .....	46
Medical Grade Epoxy Mixture:.....	49
Gelatin .....	49
Ultrasound Testing .....	49
Appendix C: Data Processing Code.....	51
Main Stack Analysis MATLAB Code .....	51
Main Discs Analysis MATLAB Code .....	57
Stacks Results to Excel MATLAB Code .....	61
Individual Disc Results to Excel MATLAB Code .....	62
Statistical Analysis SAS Code .....	65

## List of Figures

Figure 1: Electric Potential Generated by Bone Under Mechanical Load .....	8
Figure 2: Piezoelectric Effect .....	8
Figure 3: Piezoelectric Material Dipole Moments A) Before Poling B) During Poling C) After Poling – Adapted from APC International, Ltd. ....	9
Figure 4: Schematic Illustration of Axis Orientations .....	10
Figure 5: Illustration of 33 Mode.....	10
Figure 6: Monolithic versus Stacked Piezoelectric Elements – Adapted from Platt et al. ....	11
Figure 7: Average Power Across Load Resistance for Stacked and Monolithic Elements - Adapted from Platt et al. ....	12
Figure 8: Responses to Applied Ultrasound Waves – A) Attenuation, B) Scattering, C) Reflection, and D) Absorption – Adapted from Falyar .....	14
Figure 9: Encapsulation Design Schematic for 0.0 mm (Left) and 0.8 mm (Right) Compliant Layer Thicknesses ....	28
Figure 10: Application Angle Variations a) 0 degrees, b) 45 degrees, c) 90 degrees .....	30
Figure 11: Average Power Across the Resistance Sweep for Varying Ultrasound Intensities. Compliant Layer Thickness and Application Angle of: A) 0.0 mm & 0°, B) 0.8 mm & 0°, C) 0.0 mm & 45°, D) 0.8 mm & 45°, E) 0.0 mm & 90°, F) 0.8 mm & 90° .....	32
Figure 12: Average Maximum Power versus Application Angle (Intensity = 0.5 W/cm <sup>2</sup> ) .....	33
Figure 13: Contributions of Individual Disc Voltages Tested at 0 Degrees with a compliant layer thickness of: A) 0.0 mm and B) 0.8 mm .....	34
Figure 14: Average Power Across the Resistance Sweep for Varying Ultrasound Intensities. Compliant Layer Thickness and Application Angle of: A) 0.0 mm & 0.8 mm 0°, B) 0.0 mm & 0.8 mm 45°, C) 0.0 mm & 0.8 mm 90° .....	42
Figure 15: Average Power Across the Resistance Sweep for Varying Application Angles. Compliant Layer Thickness and Intensity of: A) 0.0 mm & 0.1 W/cm <sup>2</sup> , B) 0.8 mm & 0.1 W/cm <sup>2</sup> , C) 0.0 mm & 0.5 W/cm <sup>2</sup> , D) 0.8 mm & 0.5 W/cm <sup>2</sup> , E) 0.0 mm & 1.0 W/cm <sup>2</sup> , F) 0.8 mm & 1.0 W/cm <sup>2</sup> .....	43
Figure 16: Average Power Across the Resistance Sweep for Varying Application Angle. Compliant Layer Thickness and Intensity of: A) 0.0 mm & 0.8 mm, 0.1 W/cm <sup>2</sup> , B) 0.0 mm & 0.8 mm, 0.5 W/cm <sup>2</sup> , C) 0.0 mm & 0.8 mm, 1.0 W/cm <sup>2</sup> .....	44
Figure 17: Average Maximum Power versus Application Angle Compliant Layer Thickness and Intensity of: A) 0.0 mm & 0.8 mm 0.1 W/cm <sup>2</sup> , B) 0.0 mm & 0.8 mm 0.5 W/cm <sup>2</sup> , C) 0.0 mm & 0.8 mm 1.0 W/cm <sup>2</sup> .....	45

## List of Tables

Table 1: Classification of Ultrasound Heating Effects Based on Temperature .....	17
Table 2: Maximum Power Output for 0.0 mm and 0.8 mm Compliant Layer Thicknesses .....	33

## List of Equations

Equation 1: Tissue Temperature Increase Model .....	17
Equation 2: RMS Voltage.....	30
Equation 3: Power Calculation .....	30



## Chapter 1: Introduction

### 1.1 Background and Motivation

It is estimated that over the course of one's lifetime they will suffer from at least two fractured bones [2]. Two of the most common orthopedic surgeries performed are for fracture repair and fusion [3]. These surgeries are performed to immobilize, support, and set the break increasing the chance of healing through bone remodeling. Unfortunately, not all surgeries end in a success with 5-10% failing to fuse, often referred to as a non-union [4]. If a non-union occurs then a secondary surgery is often required, but it may not increase the chances of fusion [5]. Non-unions are most often seen in tobacco users, diabetics, and elderly individuals but can also be the result of an infection or severe break. Adjunct therapies, such as bone stimulators, are available and have been shown to increase the rate of healing [6]. Direct current (DC) electrical stimulation is one of the more common modes used in bone stimulators and has been successful, but this mode of stimulation requires surgical implantation of electrodes which are powered by a battery pack. One major down side to this type of therapy is that batteries are constrained by their limited lifespan and a secondary surgery is required for replacement or removal.

Piezoelectric materials (such as lead-zirconate-titanate, or PZT) used as power generators have gained popularity in bone stimulation applications as they are self-powered and do not require a battery. When a mechanical load is applied to the material an electrical potential is generated, referred to as the piezoelectric effect. Unfortunately, these materials in their natural state exhibit poor source characteristics, such as high source impedance and low power output, making them difficult to develop for these applications. Through modifications to the materials, research has shown that these negative characteristics can be minimized, making piezoelectric materials feasible for use in bone stimulation. Much of the current research using PZT for bone stimulation relies on physiological loading to stimulate the PZT, but this is not always practical. If an individual is classified as non-weight bearing, such as in the case of a highly comminuted fracture, then other means of loading are necessary for these materials to work.

Meanwhile, ultrasound therapies are known for their ability to safely interact with the internal structures of the body. One such interaction is the ability to mechanically load structures through the energy transfer of high frequency sound waves. The use of this therapy could be a way of simulating physiological loads necessary to activate the PZT.

## 1.2 Specific Aims

The main purpose of this study was to determine the efficacy of using therapeutic ultrasound to stimulate piezoelectric composite materials used in power generation applications. This was accomplished by investigating the effect of (1) ultrasound intensity (0.1 W/cm<sup>2</sup>, 0.5 W/cm<sup>2</sup>, 1.0 W/cm<sup>2</sup>), (2) thickness of compliant layers (0.0 mm, 0.8 mm), and (3) application angle (0°, 45°, 90°) on power generation. Additional measurements were collected with relation to individual PZT disc output, differing from the above measures that were collected as a complete stack. This information was used to understand the contribution and effectiveness of each disc to aid in future design decisions. It was hypothesized that: (1) an increase in ultrasound intensity would result in an increase power output, (2) the larger compliant layer thickness would exhibit the largest power generation amongst all conditions, and (3) the 0° testing condition would exhibit the highest power generation when compared to alternate angles. It was also hypothesized, for individual disc measurements, that the voltage produced by each disc would decrease the further they are from the ultrasound transducer.

## Chapter 2: Background and Literature Review

This chapter introduces the background information necessary for this study, and reviews current literature in the field.

### 2.1 Bone Remodeling and Healing

The human body is composed of several systems working together to satisfy a common goal. For example, the skeletal system, comprised of hundreds of bones, is responsible for structure and stability. Bone can be described as a dynamic tissue, as it is continuously changing over time as a response to mechanical and physiological environmental changes. When bone undergoes an adaptive change, whether it is developing new bone, maintaining old bone, or repairing damaged bone, it is referred to as remodeling [7]. The remodeling process is often the result of the conversion of an applied mechanical load to a biochemical signal, initiating a cellular response, also known as mechanotransduction [8]. Overall these processes aid in maintaining bone mass and minimizing fracture risk by constantly regulating bone structure [7, 9].

#### 2.1.1 Wolff's Law

The idea that bone remodeling and adaptation occur in response to its environment was observed as early as the 16<sup>th</sup> century, but science often credits the idea to Julius Wolff and the development of Wolff's Law [7]. Julius Wolff was a German surgeon who, in 1892, published "The Law of Bone Transformation" summarizing his earlier work. Wolff relates his findings to that of a mathematical model, stating "alterations of the internal architecture clearly observed and following mathematical rules, as well as secondary alterations of the external form of the bone following the same mathematical rules, occur as a consequence of primary changes in the shape and stressing or in the stressing of the bones" [10, 11]. Wolff's Law is not without controversy, stating it neglects both biological and engineering ideas, but all can agree that there is a link between mechanical loading and bone formation. Wolff's original ideas have served as a precursor over time and Wolff's law has

been further expanded to include: strength optimization, trabeculae alignment with the direction of principal stress, and bones ability to self-regulate in response to mechanical loading [7].

### 2.1.2 The Wnt Pathway

The relationship between mechanical loading and bone remodeling is well researched and understood, but the biological and cellular mechanism responsible for the bone remodeling processes are not as understood. On a cellular level much of our previous understanding revolved around osteoblasts and osteoclasts for their roles in bone formation and resorption, and osteocytes for their role in mechanosensing. Recently, the Canonical Wnt signaling pathway has gained attention for its involvement in the bone remodeling process and how it relates to osteocytes. For cells to sense and respond to changes in their environment they must be able to communicate these changes, this is the role of signaling pathways. Surface receptors are found on the cell membrane and they allow external proteins to bind and initiate some internal cellular response, known as signal transduction. The Wnt protein is responsible for initiating the Wnt signaling pathway by binding to surface receptors, resulting in an increase in  $\beta$ -catenin within the cell [12]. Increased levels of  $\beta$ -catenin will move into the mitochondria, activating transcription factors, resulting in cell growth, proliferation and ultimately bone formation [12, 13].  $\beta$ -catenin is a protein known for its regulation of osteoblasts [12]. This process is often observed when a mechanical load is applied to bone, due to the resulting down regulation of the inhibitory protein sclerostin [13, 14]. Sclerostin can bind to surface receptors in place of Wnt proteins, resulting in an inactivation of the Wnt signaling pathway [13]. This inactivation results in  $\beta$ -catenin degradation and increased bone resorption.

Although there is still much more to understand about the processes involved in bone remodeling, the current information has allowed researchers and medical professionals to investigate adjunct therapies to aid in the bone remodeling process. Two examples of this are the use of DC stimulation and therapeutic ultrasound as bone stimulation therapies, which are both further described below. Research on these topics is ongoing but it is believed that there may be a relation between the

positive charge of sclerostin and the electrical field generated through DC stimulation, while the heating effects of ultrasound may also help to induce the Wnt pathway [15, 16].

### 2.1.3 Compromised Bone

When bone is healthy, it is assumed that remodeling will occur naturally. Although this is true most of the time, there may be an impairment in remodeling ability, that may result in a decreased ability for the fracture to heal properly. A fracture is when a bone breaks as a result of an overload in functional capacity, a traumatic event, or bone disease [17]. Fractures can range from a thin crack to a complete break into multiple pieces [18]. If a fracture occurs in someone suffering from an impairment, then the fracture may fail to fuse naturally, resulting in delayed union, non-union, or pseudarthrosis. When a healing fracture is still progressing but at a much slower rate than anticipated it is classified as a delayed union [7]. If the fracture fails to heal it then becomes a non-union and non-unions typically result in pseudarthrosis, also known as a false joint [7]. Impairments in bone remodeling ability can often be a result of tobacco use, old age, disease, diabetes, infection, or a severe break [5]. According to the Cleveland Clinic there are over a million fractures each year in the United States, and approximately 5-10% of those will result in nonunion [1, 4]. Delayed or non-unions can have a significant impact on a patient's life as they usually result in increased costs, an increased number of surgeries, pain, and swelling; as well as limited use of that area, psychosocial disabilities, and inability to work [19]. Therefore, there is an immense need for a fracture healing aide that can help decrease the occurrence of non-union.

### 2.1.4 Bone Stimulators

Several physical and biological aides have been developed to decrease the risk of non-union in fracture patients. Some examples of biological aides include internal accelerating agents, such as bone morphogenic proteins (BMPs), and methods of bone grafting, which are subject to their own constraints [20]. The most common form of physical aides currently on the market are bone stimulators, which may be internally or externally applied. Ultimately, bone stimulators use a

physical method of stimulation, such as extracorporeal shock waves, ultrasound waves, or electrical and electromagnetic fields to stimulate bone healing [21].

Extracorporeal shock wave (ESW) stimulation is administered externally by applying pressure waves to the treated area. As these pressure waves propagate through the body, tissues undergo rapid fluctuations in positive and negative pressure, stimulating a biological response [22]. The most commonly known uses of ESW therapy are to treat kidney stones, planar fasciitis, forms of tendonitis, tennis elbow, and other chronic tendinopathies [23]. Extracorporeal shock waves have been clinically used as early as 1980 but are relatively new and less understood in the bone stimulation field. Although less understood, the idea behind using ESW for bone stimulation is to stimulate osteoblastic cells to initiate osteogenesis [24].

The use of ultrasound for bone stimulation is well known amongst scientific and clinical communities, although it is not universally accepted. Low intensity pulse ultrasound (LIPU), used in bone stimulators, is externally administered and utilizes high frequency, low intensity, pulsed sound waves that travel through tissues creating a mechanical stress. The principals behind ultrasound are explained in further detail in section 3. Currently marketed ultrasound stimulators have been in circulation for over 20 years and include one group of preset ultrasound parameters (frequency, duty cycle, and intensity). The reason behind this single set of parameters was to ensure minimal thermal effects were produced. Although studies focusing on the effects of ultrasound on bone growth started in the 1900s, they have focused specifically on rabbit femurs, analyzing the effects of intensity and frequency. A study performed by Tsai et al. used therapeutic ultrasound to investigate the effects of intensity and treatment time on bone formation in a rabbit femur [25]. When tested at a frequency of 1.5 MHz, intensities of 0.5 W/cm<sup>2</sup> and 1.0 W/cm<sup>2</sup>, and treatment times of 5, 15, and 25 minutes investigators found that intensities of 0.5 W/cm<sup>2</sup> accelerated bone formation and 1.0 W/cm<sup>2</sup> suppressed formation [25]. Reher et al. conducted a similar study investigating the effect of intensity (0.1 W/cm and 2.0 W/cm<sup>2</sup>) on bone growth stimulation as well as temperature. Results followed

previous studies stating higher intensities supported bone suppression and lower intensities supported bone formation but results of this study also suggested nonthermal effects for all intensities [26]. To clarify, the focus of this research is not to stimulate bone growth using ultrasound, but the aforementioned studies were used to establish safe parameters of ultrasound use near bone and understand alternate methods of bone stimulation.

Electrical and electromagnetic stimulators are one of the more popular methods of bone stimulation and can be administered internally and externally. These methods apply an electrical field to the treatment site generating an electrical potential similar to the piezoelectric properties found naturally in bone. Electrical stimulation can be broken down into three main techniques: noninvasive capacitive coupling (CC), noninvasive inductive coupling (IC), and invasive direct current (DC). For capacitive coupling, two electrodes are applied on either side of the bone creating an electrical potential of 1-100mV/cm across the treated area [27]. Inductive coupling creates an electrical field, of similar magnitude, in the surrounding tissues by applying a pulsed electromagnetic field (PEMF). The PEMF is generated from a current carrying coil that is applied to skin and powered by an external field generator [27]. Opposite of CC and IC techniques, direct current stimulation uses surgically implanted electrodes connected to a power supply that can either be implanted or external [28]. Research has shown that electrode implementation is crucial, placing the cathode at the stimulation site and the anode in a separate area of soft tissue [27]. Once electrodes are implanted, a direct current of 5-100 $\mu$ A can be applied directly to the treatment site [27]. Further explanation on the theory and use of DC stimulation will be explained below.

#### 2.1.5 Electrical Stimulation

The idea that electrical stimulation aids in bone healing was realized in the early 1800s with tibial fracture non-unions, but the concept was not fully understood until 1953 when Yasuda et al. described the piezoelectric properties of bone [29, 30]. This idea was further explained by Fukada et al., stating that collagen molecules exhibit piezoelectric properties, and that when bone is strained, a dipole moment is generated [29, 31]. The way that bone will respond to the generated electrical

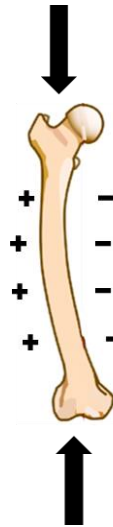


**FIGURE 1: ELECTRIC POTENTIAL GENERATED BY BONE UNDER MECHANICAL LOAD**

potential is dependent upon polarity, showing stimulation near electronegative potentials and resorption near electropositive potentials [6]. The bone in Figure 1 is an example of mechanical loading on a femur, with bone formation occurring on the right side, and resorption on the left. Several studies have built upon these ideas using DC electrical stimulation to aid in fracture healing or bone growth.

## 2.2 Piezoelectricity

### 2.2.1 Piezoelectric Effect

Materials possessing piezoelectric properties have the potential to generate an electrical charge in response to a mechanical load. This phenomenon is referred to as the piezoelectric effect Figure 2 and was first discovered in 1880, in naturally occurring crystals, by Jacques and Pierre Curie [32].

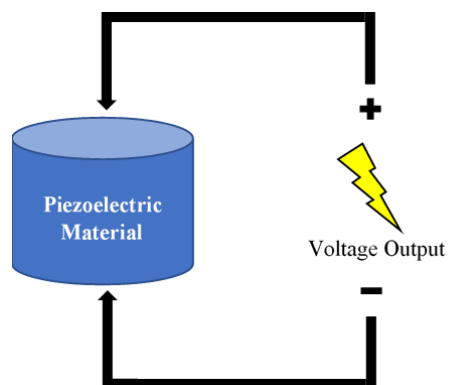


**FIGURE 2: PIEZOELECTRIC EFFECT**



The opposite effect can also occur when an electrical field is applied to the material, resulting in a deformation, referred to as the inverse piezoelectric effect.

Piezoelectric materials are comprised of crystalline structures that when deformed, result in a disruption of positive and negative ions, changing the dipole moment of the crystal and creating a net charge in the material [32, 33]. Ultimately, this change in electrical potential results in an electrical charge on opposing surfaces.

### 2.2.2 Synthetic Materials

In the 1960s man-made materials, comprising of piezoelectric ceramics such as barium titanate ( $\text{BaTiO}_3$ ) and lead-zirconate-titanate (PZT), gained popularity replacing natural piezoelectric materials. These ceramics introduced an inexpensive alternative that can be manufactured for various applications and are physically strong as well as chemically inert [32]. Although a material may contain piezoelectric properties, if the internal dipoles do not align with one another they may cancel one another out, resulting in minimal or negligible piezoelectric effects [34, 35]. Dipoles are randomly oriented naturally, but they can be forcibly aligned, to elicit a greater response, through a process called poling. Poling occurs when a strong direct current (DC) electrical field is applied to the material, causing the material to lengthen in the direction of the electrical field and aligning the

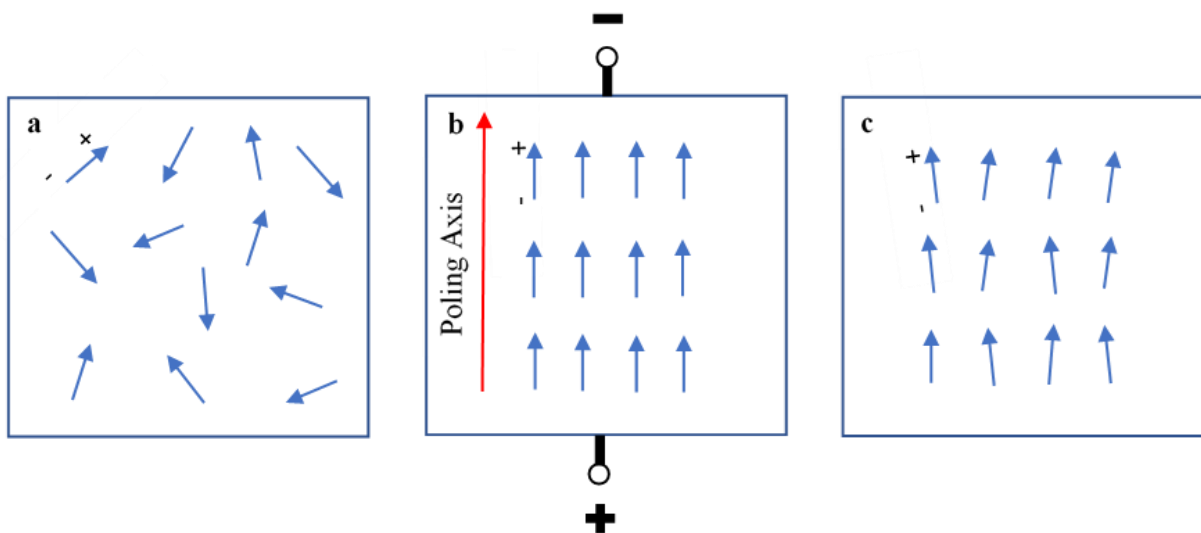


FIGURE 3: PIEZOELECTRIC MATERIAL DIPOLE MOMENTS A) BEFORE POLING B) DURING POLING C) AFTER POLING – ADAPTED FROM APC INTERNATIONAL, LTD.

dipoles [32, 35]. Once the electrical field is removed dipoles are permanently locked into place of near alignment, producing an anisotropic material [32]. This is shown in Figure 3.

### 2.2.3 Piezoelectric Constants

Since piezoelectric ceramics are anisotropic, several material properties are directionally dependent. Therefore, piezoelectric constants are used to relate various directions of the applied mechanical load or electrical field [32]. Some of the piezoelectric constants include: charge constant (d), voltage constant (g), permittivity ( $\epsilon$ ), elastic compliance (s), and electromechanical coupling factor (k) [32]. Each of these constants will have two trailing subscript numbers describing the direction of the two related measures, shown in Figure 4. The first subscript represents the poling direction and the second subscript represents the direction of mechanical loading [32].



FIGURE 4: SCHEMATIC ILLUSTRATION OF AXIS ORIENTATIONS

In the scope of this study the 33 mode was observed to understand how the material would respond in various conditions, as depicted in Figure 5. Depending on the application and desired outcome it is important to understand these constants and their related measures.

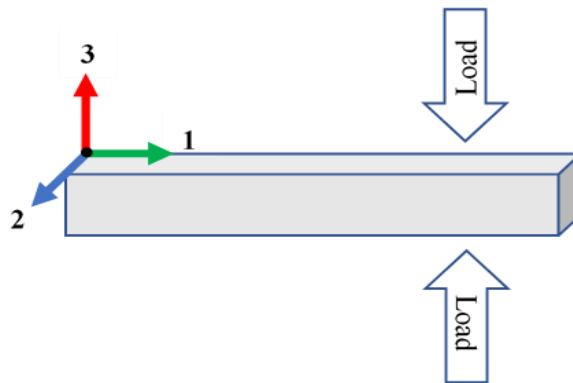


FIGURE 5: ILLUSTRATION OF 33 MODE

## 2.2.4 Applications

Piezoelectric materials are used in a wide variety of applications functioning as sensors, actuators, transducers, and generators [32]. Although the physical material used in these applications may be the same, depending on the design, the outcomes are very different. Typically, when used as a sensor, the piezoelectric material measures a physical parameter and converts it into an electrical signal. Whereas when used as an actuator, an electrical signal is measured and converted into a physical parameter. Rather than directly measuring, transducers convert electrical energy into a mechanical energy, often vibrational, expressed either audibly or as ultrasound. On the other hand, when used as a generator, the piezoelectric materials have the ability to generate voltages when stimulated by a mechanical load [32]. This study utilizes piezoelectric materials functioning as both a transducer and generator, in the form of an ultrasound transducer (probe) and fabricated test specimens.

## 2.2.5 Stacked Composites

The use of piezoelectric materials as energy harvesters and power generators is less common than their use as sensors and actuators, mainly due to the materials poor source characteristics [36]. Without modifications, these materials exhibit high voltage, low current, high impedance, and low power output [36]. Size, shape, volume, and form can determine the outcome and influence these source characteristics have on the intended application. A study by Platt et al. found that size and shape of the piezoelectric element affected power generation, but element form affects the electrical source characteristics. The form factors used in this study, shown in Figure 6, were cylindrical monolithic elements, a solid homogeneous material, and stacked elements, multiple piezoelectric

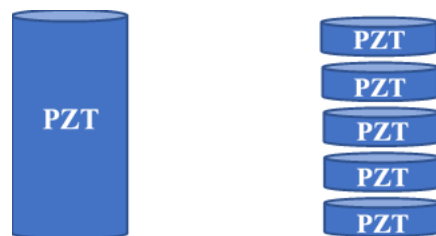


**FIGURE 6: MONOLITHIC VERSUS STACKED PIEZOELECTRIC ELEMENTS – ADAPTED FROM PLATT ET AL.**

wafers stacked together mechanically in series and electrically in parallel [37]. The power generated was the same for both form factors, but the stacked orientation decreases resistive load (impedance), decreases output voltage and increases effective capacitance when compared to the monolithic element [37]. These results are depicted in Figure 7.

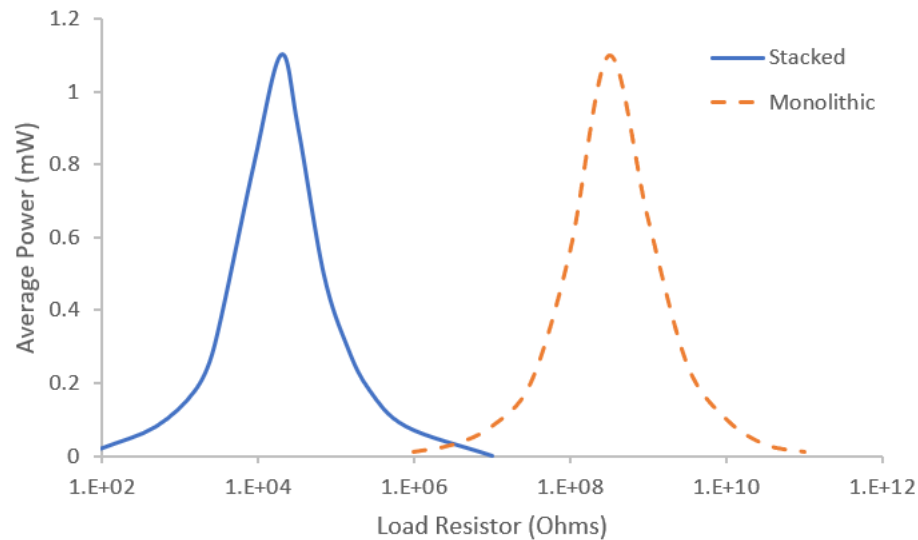


**FIGURE 7: AVERAGE POWER ACROSS LOAD RESISTANCE FOR STACKED AND MONOLITHIC ELEMENTS - ADAPTED FROM PLATT ET AL.**

Another study, performed by Goetzinger et al. observed the effect of the number of stacks, on power generation, within a stacked element form. They found that increasing the number of layers would decrease their optimal resistive load, but max power would not be significantly influenced [38].

Aside from poor source characteristics, piezoelectric ceramics are also brittle, and without modification are not ideal for mechanical loading due to high risk of failure. Piezoelectric composites, consisting of a piezoelectric ceramic and polymer mix, allow for optimized material properties, such as strength [39]. Depending on the materials used, these composites can also contain properties such as high coupling factors, material matching properties (water & tissue), low acoustic impedance, mechanical flexibility, and increased mechanical strength [39]. In this study, a

piezoelectric composite was utilized for its mechanical strength properties as an encapsulating material in order to better suit electrical/physiological functions.

Depending on the intended application, more power may be necessary and therefore, methods to amplify power generation which also utilized piezoelectric composites were explored. A study by Krech et al. looked at the effect of compliant layers, placed between piezoelectric discs within the stack, on power generation in low frequency applications. Within this study, the test specimens including compliant layers were referred to as CLACS, Compliant Layer Adaptive Composite Stacks [40]. It was concluded that specimens incorporating CLACS showed a significant increase in power production across all testing parameters while maintaining the same volume of piezoelectric material [40]. Although only performed on low frequency applications, due to the positive outcomes observed in the Krech et al. study, CLACS were incorporated into the scope of this research.

#### 2.2.6 Piezoelectric Materials in Bone Stimulation

The use of piezoelectric materials for energy harvesting and power generation applications intended to stimulate bone has recently increased in popularity. Piezoelectric power generators have proven to be advantageous because they are self-driven and do not require batteries, which are subject to limited lifespans, and typically do not require a removal surgery [41]. These power generators are self-driven through their ability to capture mechanical energy and convert it into a usable electrical charge. Several studies have investigated the effectiveness of the use of piezoelectric materials, in various configurations, for power generation and to enhance bone growth. Cochran et al. utilized monolithic piezoelectric materials in an internal fixation device and showed that voltages, within the range known to stimulate osteogenesis, could be generated under physiological (walking) and external (ultrasound) loading conditions [42]. Another study developed a spinal fusion implant with multiple stacked layers of macro fiber piezoelectric composite material [38]. This implant was later used in a pilot ovine study that incorporated it into a spinal fusion implant to generate power under a mechanical load, delivering DC stimulation to an electrode placed

near the fusion site [43]. This study showed that levels of DC stimulation that were sufficient to enhance bone growth could be generated from the spinal implant [38, 43]. Each of these studies suggest that there is a large potential for the use of piezoelectric materials in bone stimulation applications and they should be explored further.

### 2.3 Ultrasound

When sound waves exceed a frequency of 20 kHz, they are no longer audible to the human ear and are then classified as ultrasound. Ultrasound waves consist of mechanical sound waves traveling through various mediums at frequencies ranging from 20 kHz-20 MHz [44]. Applications range from nondestructive testing in the industrial field to diagnostic imaging, therapeutic treatments, and tissue ablation in the medical field.

Ultrasound transducers are comprised of multiple piezoelectric elements that are used to convert electrical energy into mechanical energy. When electrical energy is applied across piezoelectric elements it causes them to deform, creating the ultrasonic sound waves. Once these waves are generated and applied, they can either attenuate, scatter, reflect, or absorb [45]. These are shown in Figure 8. All signals will attenuate but the rate at which this occurs will depend on the distance traveled, medium its traveling through, and strength of the overall signal. Scattering occurs when the

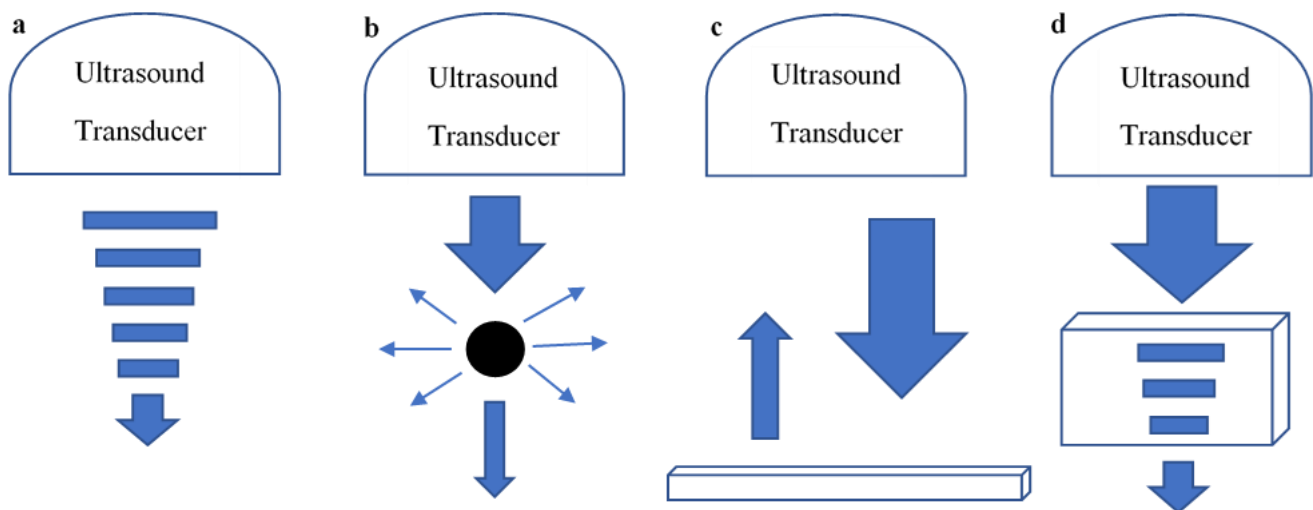


**FIGURE 8: RESPONSES TO APPLIED ULTRASOUND WAVES – A) ATTENUATION, B) SCATTERING, C) REFLECTION, AND D) ABSORPTION – ADAPTED FROM FALYAR**

wavelength of the ultrasound signal is larger than the item it contacts. This is commonly seen in medical use with red blood cells and results in the signal being scattered in all directions with little to no returned reflection. Reflection is most often used in medical imaging and primarily results from signal transmission through two mediums of varying impedances. When the signal reaches this boundary, a portion of the wave will continue through the boundary while the remaining portion will reflect towards the transducer. Two well-known tissues with varying impedance values are soft tissue and bone. Lastly, absorption is an energy transfer from the ultrasound wave to the treated tissue, most often used in a therapeutic setting for heating [45]. While each of these outcomes are unique, they all may occur in some capacity when ultrasound is used.

### 2.3.1 Ultrasound Parameters

Ultrasound is most effective when the necessary parameters are set for the intended application; these parameters include frequency, duty cycle, and intensity. Ultrasound frequency, measured in Hertz, characterizes the number of sound waves emitted per second and is inversely related to wavelength [46]. Higher frequencies are used for higher imaging resolution but have a lower penetration depth. On the other hand, low frequencies are utilized when a deeper penetrating wave is necessary, but this results in a lower imaging resolution [47]. Often frequencies are chosen to achieve the most optimal result but there are times it is beneficial to compromise between the two. Depending on the desired dosage, ultrasound can be applied continuously or pulsed by varying the duty cycle. Often represented as a percentage, duty cycle is the ratio of on/off time of applied ultrasound and is varied to best fit the desired outcome. For example, if an increased intensity was needed without inducing thermal effects, then a pulsed duty cycle may be used. Ultrasound intensity is most commonly expressed in terms of  $W/cm^2$ , describing the power delivered in relation to the area across which it is distributed [48]. Energy transfer is directly related to ultrasound intensity, the higher the intensity, the greater the energy transfer. High intensities are typically used in surgery and cancer treatments, whereas low intensities are often used in diagnostic and therapeutic settings.

Intensities below  $3 \text{ W/cm}^2$  are referred to as low intensity, and intensities above  $3 \text{ W/cm}^2$  are referred to as high intensity [49].

### 2.3.2 Diagnostic versus Therapeutic Ultrasound

Medical ultrasound is a general term referring to ultrasound used in a medical setting, but there are different focuses across medical fields where ultrasound is used. Although the mode in which ultrasound waves are generated is the same, the parameters and outcome can differ. Therefore, medical ultrasound will be discussed in terms of diagnostic and therapeutic approaches.

Diagnostic ultrasound is a safe and noninvasive technique used to generate a real time image of subcutaneous structures of the body [50]. Typically, diagnostic ultrasound is performed for an anatomical or functional purpose. Anatomical ultrasound is used only to image internal organs and structures, but functional ultrasound incorporates physical characteristics, such as movement, fluid flow, and stiffness, into the image [51]. For an image to be produced, ultrasound waves must reflect off bodily structures and travel back to the transducer for transmission. By fine tuning the ultrasound parameters, the image can be adjusted, and different areas of the human body can be examined. Diagnostic ultrasound parameters most commonly consist of frequencies ranging from 1-20 MHz, pulsed or continuous duty cycles, and intensities that typically range from  $0.05\text{-}0.5 \text{ W/cm}^2$  [49]. While the range for each parameter is relatively large, there are FDA regulations for diagnostic ultrasound that provide an outline of acceptable parameters based on the intended application. For example, when used for fetal, cardiac, or peripheral vessel imaging, the intensity cannot exceed  $94 \text{ mW/cm}^2$ ,  $430 \text{ mW/cm}^2$ , and  $720 \text{ mW/cm}^2$ , respectively [52]. These regulations are to ensure that unintended effects, such as heating or cavitation, do not occur.

Unlike diagnostic ultrasound, the purpose of therapeutic ultrasound is not to generate an image but to physically interact with internal structures and tissues instead. Ultrasound waves are mechanical sound waves; therefore, they can be used for modification purposes such as moving/pushing contacted objects, to dissolve blood clots, heat tissue, and aid in drug delivery, as



well as destructive purposes such as tissue ablation [44]. Ultimately, therapeutic ultrasound is categorized by the resulting biophysical effect: thermal or nonthermal. Thermal effects, the resultant of heating, include increased blood flow, metabolic activity, extensibility, and reduced pain. Nonthermal effects include mechanical stress, cavitation, and gas activation [44]. If thermal effects are the desired outcome, literature has shown that the internal temperature must reach a temperature of 40-45°C [53, 54]. A study performed by Lehman et al. showed that, with a base temperature of 36-37°C, the level of heating and application can be classified by temperature increases as seen in Table 1 [54, 55].

**TABLE 1: CLASSIFICATION OF ULTRASOUND HEATING EFFECTS BASED ON TEMPERATURE**

<b>Level of Heating</b>	<b>Temperature Increase</b>	<b>Application</b>
Mild	1°C	Increased metabolic activity
Moderate	2-3°C	Reduction of pain and inflammation, as well as increased blood flow
Vigorous	>4°C	Used for stretching due to the alteration in viscoelastic properties

For any interaction to occur, the ultrasound signal needs to both reach and interact with the desired tissue, through vibration or absorption. The resultant outcomes are heavily dependent upon how the ultrasound parameters are configured. Draper et al. presented a formula to describe the relationship between ultrasound parameters and tissue temperature increase. When studying the effect of frequency, intensity, and treatment time on human tissue, Draper used Equation 1 as a theoretical model to anticipate tissue temperature increase [53, 54]. Therapeutic ultrasound parameters typically consist of frequencies ranging from 20 kHz-3 MHz, pulsed or continuous duty cycles, and intensities ranging from 0.03-1,000 W/cm<sup>2</sup> [49].

$$0.2^{\circ}\text{C} \times \text{treatment time (minutes)} \times \text{intensity} \left( \frac{\text{W}}{\text{cm}^2} \right) = \text{temperature increase } (^{\circ}\text{C})$$

**EQUATION 1: TISSUE TEMPERATURE INCREASE MODEL**

Overall, the field of medical ultrasound is dependent on how ultrasound waves interact with the body and the biological effects that are produced as a result. These biological effects (bioeffects), in general, are neither good nor bad. A certain outcome may be considered beneficial in some

applications, but detrimental in others. For example, tissue heating is a beneficial bioeffect when utilized in certain therapeutic ultrasound applications, such as increasing the blood flow and decreasing inflammation to an injury site. On the other hand, when ultrasound is being used to conduct a sonogram and examine a fetus, tissue heating would be considered a negative bioeffect. By understanding how the ultrasound signal will interact with the human body, the intended application, and how to correctly tune the ultrasound parameters, medical professionals can take advantage of this incredible tool to produce the most beneficial outcome.

For this research study, therapeutic ultrasound was chosen for several reasons. First off, producing an image from the ultrasound equipment was not necessary. The main goal was to merely apply a mechanical load to the specimen, not to view internal structures. Additionally, using therapeutic ultrasound allowed the research team more flexibility to vary the ultrasound parameters and investigate their effects on power production. It is still possible to vary the parameters with diagnostic ultrasound, but typically the equipment is designed with a certain application in mind, so parameters such as intensity and frequency are much more difficult to adjust. Modifying these parameters would typically require changing the equipment, instead of changing a setting on the ultrasound machine. Lastly, therapeutic ultrasound machines are much more accessible and typically are lower cost than diagnostic ultrasound machines.

## 2.4 Tissue Mimicking Phantoms

As technology advances, it is important to understand how medical devices interact with biological systems. Various synthetic materials, referred to as tissue mimicking phantoms, have been developed to represent important properties found human tissue. These tissue mimicking phantoms (TMP) are a low-cost alternative allowing researchers and clinicians to perform testing, training, calibration, and validation in a safe environment [56].

Ultrasound technology is a field that benefits from TMPs due to the large number of varying applications. Depending on the desired application, models must be tested to understand acoustic,

mechanical, and thermal properties. Therefore, using a medium that mimics soft tissue properties is essential. Generally, ultrasound TMPs are used to mimic acoustic properties of tissue such as speed of sound and attenuation, as well as mimic sonographic appearance of tissue [57]. Although there are some options commercially available for purchase, TMPs can also be homemade using various gelatinous materials. Quarsh et al. used unflavored gelatin powder, evaporated milk, cornstarch, Dettol antiseptic liquid, and food coloring to create a biopsy and vascular TMP used for interventional radiology training [58]. A different study by Richardson et al., focused on fine needle aspiration, created a TMP using Knox unflavored gelatin powder, psyllium husk fiber powder, food coloring, as well as olives and blueberries used to represent tissue masses [56]. Gelatinous materials are used to create a soft tissue like material, mimicking properties like mechanical stiffness. Other items such as corn starch, evaporated milk, or fibers were added for an echogenic effect often seen in imaging. Lastly blueberries, olives, and other foreign materials were added to mimic masses like tumors. Both commercial and homemade TMPs are beneficial amongst the ultrasound community for their adjustable characteristics and ability to provide a low-cost mode of research and an ethical means of training for students and clinicians.

## 2.5 References

1. Cleveland Clinic. *Bone Fractures*. 2017; Available from: <https://my.clevelandclinic.org/health/diseases/15241-bone-fractures>.
2. National Ambulatory Medical Care Survey & American Academy of Orthopaedic. *Fractures/Broken Bones Data*. Available from: [https://www.schwebel.com/userfiles/files/Fractures\(1024\).pdf](https://www.schwebel.com/userfiles/files/Fractures(1024).pdf).
3. Marina Del Ray Hospital. *What are the most common orthopedic surgeries?* 2019; Available from: <https://www.marinahospital.com/faq/what-are-the-most-common-orthopedic-surgeries>.
4. Zura, R., et al., *Epidemiology of Fracture Nonunion in 18 Human Bones*. JAMA Surg, 2016. **151**(11): p. e162775.
5. American Academy of Orthopedic Surgeons. *Nonunions*. Diseases & Conditions 2014; Available from: <https://orthoinfo.aaos.org/en/diseases--conditions/nonunions/>.
6. Rubinacci, A., et al., *Changes in bioelectric potentials on bone associated with direct current stimulation of osteogenesis*. J Orthop Res, 1988. **6**(3): p. 335-45.
7. Martin, R.B., D.B. Burr, and N.A. Sharkey, *Skeletal tissue mechanics*. 1998, New York: Springer. xiv, 392 p.
8. Huang, C. and R. Ogawa, *Mechanotransduction in bone repair and regeneration*. FASEB J, 2010. **24**(10): p. 3625-32.
9. Weinkamer, R., C. Eberl, and P. Fratzl, *Mechanoregulation of Bone Remodeling and Healing as Inspiration for Self-Repair in Materials*. Biomimetics (Basel), 2019. **4**(3).
10. Ruff, C., B. Holt, and E. Trinkaus, *Who's afraid of the big bad Wolff?: "Wolff's law" and bone functional adaptation*. Am J Phys Anthropol, 2006. **129**(4): p. 484-98.
11. Wolff, J., *The Law of Bone Remodelling*. 1986: Springer-Verlag Berlin Heidelberg. 126.
12. Chen, J. and F. Long, *beta-catenin promotes bone formation and suppresses bone resorption in postnatal growing mice*. J Bone Miner Res, 2013. **28**(5): p. 1160-9.
13. Galea, G.L., L.E. Lanyon, and J.S. Price, *Sclerostin's role in bone's adaptive response to mechanical loading*. Bone, 2017. **96**: p. 38-44.
14. Robling, A.G., et al., *Mechanical stimulation of bone in vivo reduces osteocyte expression of Sost/sclerostin*. J Biol Chem, 2008. **283**(9): p. 5866-75.
15. Veverka, V., et al., *Characterization of the structural features and interactions of sclerostin: molecular insight into a key regulator of Wnt-mediated bone formation*. J Biol Chem, 2009. **284**(16): p. 10890-900.
16. Olkku, A., et al., *Ultrasound-induced activation of Wnt signaling in human MG-63 osteoblastic cells*. Bone, 2010. **47**(2): p. 320-30.
17. American Academy of Orthopedic Surgeons. *Fractures (Broken Bones)*. Diseases & Conditions 2012; Available from: <https://orthoinfo.aaos.org/en/diseases--conditions/fractures-broken-bones/>.
18. Giorgi, A.Z. *Fracture*. 2016; Available from: <https://www.healthline.com/health/fracture>.
19. Tay, W.H., et al., *Health outcomes of delayed union and nonunion of femoral and tibial shaft fractures*. Injury, 2014. **45**(10): p. 1653-8.
20. Lissenberg-Thunissen, S.N., et al., *Use and efficacy of bone morphogenetic proteins in fracture healing*. Int Orthop, 2011. **35**(9): p. 1271-80.
21. Wienke, J. and P. Payton, *Bone Stimulation For Nonunions: What The Evidence Reveals*. Podiatry Today, 2011. **24**(9): p. 52-57.
22. Notarnicola, A. and B. Moretti, *The biological effects of extracorporeal shock wave therapy (eswt) on tendon tissue*. Muscles Ligaments Tendons J, 2012. **2**(1): p. 33-7.
23. *What Conditions can be Treated by ESWT?* Excellence Shock Wave Therapy: FAQs 2019; Available from: <https://www.eswtusa.com/faqs#question5>.
24. Moretti, B., et al., *Bone healing induced by ESWT*. Clin Cases Miner Bone Metab, 2009. **6**(2): p. 155-8.

25. Tsai, C.L., W.H. Chang, and T.K. Liu, *Preliminary studies of duration and intensity of ultrasonic treatments on fracture repair*. Chin J Physiol, 1992. **35**(1): p. 21-6.
26. Reher, P., et al., *The stimulation of bone formation in vitro by therapeutic ultrasound*. Ultrasound Med Biol, 1997. **23**(8): p. 1251-8.
27. Aaron, R.K., D.M. Ciombor, and B.J. Simon, *Treatment of nonunions with electric and electromagnetic fields*. Clin Orthop Relat Res, 2004(419): p. 21-9.
28. BlueCross BlueShield of North Carolina, *Electrical Bone Growth Stimulation - Corporate Medical Policy*. 2019.
29. Onibere, R. and A. Khanna, *The Role Of Electrical Stimulation In Fracture Healing*. The Internet Journal of Orthopedic Surgery, 2008. **11**.
30. Yasuda, I., *Piezoelectricity of Living Bone*. Journal of Kyoto Prefectural University of Medicine, 1953. **53**(325).
31. Fukada, E. and I. Yasuda, *On the Piezoelectric Effect of Bone*. Journal of the Physical Society of Japan, 1957. **12**(10): p. 5.
32. APC International, L., *Piezoelectric Ceramics: Principles and Applications*. 2011: APC International.
33. Unknown, *Chapter 2: Background*. Virginia Tech. p. 14.
34. Dahiya, R.S. and M. Valle, *Fundamentals of Piezoelectricity*, in *Robotic tactile sensing : technologies and system*. 2013, Springer: Dordrecht ; New York. p. 195-210.
35. Jaffe, B., W.R. Cook, and H.L. Jaffe, *Piezoelectric ceramics*. Non-metallic solids,. 1971, London, New York,: Academic Press. ix, 317 p.
36. Nayan, H., *Power Generation Using Piezoelectric Material*. Journal of Material Sciences & Engineering, 2015. **4**(3): p. 1-4.
37. Platt, S.R., S. Farritor, and H. Haider, *On low-frequency electric power generation with PZT ceramics*. IEEE/ASME Transactions on Mechatronics, 2005. **10**(2): p. 240-252.
38. Goetzinger, N.C., et al., *Composite piezoelectric spinal fusion implant: Effects of stacked generators*. J Biomed Mater Res B Appl Biomater, 2016. **104**(1): p. 158-64.
39. Uchino, K., *Chapter 9 - Piezoelectric Composite Materials*, in *Advanced Piezoelectric Materials (Second Edition)*, K. Uchino, Editor. 2017, Woodhead Publishing. p. 353-382.
40. Krech, E.D., et al., *Effect of compliant layers within piezoelectric composites on power generation providing electrical stimulation in low frequency applications*. J Mech Behav Biomed Mater, 2018. **88**: p. 340-345.
41. Li, H., C. Tian, and Z.D. Deng, *Energy harvesting from low frequency applications using piezoelectric materials*. Applied Physics Reviews, 2014. **1**(4): p. 041301.
42. Cochran, G.V., et al., *Piezoelectric internal fixation devices: a new approach to electrical augmentation of osteogenesis*. J Orthop Res, 1985. **3**(4): p. 508-13.
43. Friis, E.A., S.N. Galvis, and P.M. Arnold, *DC Stimulation for Spinal Fusion with a Piezoelectric Composite Material Interbody Implant: An Ovine Pilot Study*. 2015.
44. Ahmadi, F., et al., *Bio-effects and safety of low-intensity, low-frequency ultrasonic exposure*. Prog Biophys Mol Biol, 2012. **108**(3): p. 119-38.
45. Falyar, C.R. *Reflection, Refraction, Scattering, and Attenuation*. Ultrasound Physics 2017; Available from: <https://www.vaulttrasound.com/educational-resources/ultrasound-physics/reflection-refraction/>.
46. Abu-Zidan, F.M., A.F. Hefny, and P. Corr, *Clinical ultrasound physics*. J Emerg Trauma Shock, 2011. **4**(4): p. 501-3.
47. Tsaklis PhD, P., *Presentation of Acoustic Waves Propagation and Their Effects Through Human Body Tissues*. Human Movement, 2010. **11**.
48. DJO Global, *Intelect Transport Combo Units User Manual*. 2010, DJO Global LLC: Vista, California, USA.
49. Xin, Z., et al., *Clinical applications of low-intensity pulsed ultrasound and its potential role in urology*. Transl Androl Urol, 2016. **5**(2): p. 255-66.

50. Lucas, V.S., et al., *Utility of high-frequency ultrasound: moving beyond the surface to detect changes in skin integrity*. *Plast Surg Nurs*, 2014. **34**(1): p. 34-8.
51. National Institute of Biomedical Imaging and Bioengineering. *Ultrasound*. 2016; Available from: <https://www.nibib.nih.gov/science-education/science-topics/ultrasound>.
52. Vaezy, S. and K. Wear, *Marketing Clearance of Diagnostic Ultrasound Systems and Transducers*, U.S. Food and Drug Administration, Editor. 2019.
53. Kimura, I.F., et al., *Effects of two ultrasound devices and angles of application on the temperature of tissue phantom*. *J Orthop Sports Phys Ther*, 1998. **27**(1): p. 27-31.
54. Draper, D.O., J.C. Castel, and D. Castel, *Rate of temperature increase in human muscle during 1 MHz and 3 MHz continuous ultrasound*. *J Orthop Sports Phys Ther*, 1995. **22**(4): p. 142-50.
55. Lehmann, J.F., et al., *Heating produced by ultrasound in bone and soft tissue*. *Arch Phys Med Rehabil*, 1967. **48**(8): p. 397-401.
56. Richardson, C., S. Bernard, and V.A. Dinh, *A Cost-effective, Gelatin-Based Phantom Model for Learning Ultrasound-Guided Fine-Needle Aspiration Procedures of the Head and Neck*. *J Ultrasound Med*, 2015. **34**(8): p. 1479-84.
57. Bude, R.O. and R.S. Adler, *An easily made, low-cost, tissue-like ultrasound phantom material*. *J Clin Ultrasound*, 1995. **23**(4): p. 271-3.
58. Qurash, M.T., et al., *Special Ultrasound Phantom for Interventional Training: Construction, Advantages, and Application*. *J Med Ultrasound*, 2018. **26**(4): p. 210-214.

### Chapter 3: Journal of Medical Devices Research Paper (In Progress)

This section contains a manuscript to be submitted for publication with the Journal of Medical Devices.

## **Determination of Clinical Efficacy of Ultrasound Stimulation on Piezoelectric Composites for Power Generation Applications**

Authors:

### **Morghan Alters**

Spine Biomechanics Laboratory,  
Department of Bioengineering,  
University of Kansas,  
Lawrence, KS 66045  
Email: mkalters@ku.edu

### **Ember Krech**

Spine Biomechanics Laboratory,  
Department of Bioengineering,  
University of Kansas,  
Lawrence, KS 66045  
Email: ekrech@ku.edu

### **Linda D'Silva**

Clinical Assistant Professor  
Department of Physical Therapy and Rehabilitation Science,  
University of Kansas Medical Center,  
Kansas City, KS 66160  
Email: ldsilva@kumc.edu

### **Elizabeth Friis\***

Professor,  
Department of Mechanical Engineering,  
University of Kansas,  
Lawrence, KS 66045  
Email: lfriis@ku.edu

\* Corresponding Author

### 3.1 Abstract

Fracture repair and fusion account for two of the most common orthopedic surgical procedures [1]. If these surgeries are unsuccessful, the bone may fail to fuse and is classified as a nonunion, which is life altering. Adjunct therapies, such as bone stimulators, are available to aid in bone healing but these methods require patient compliance or battery packs. Piezoelectric composite materials have shown promising results as self-powered generators in bone stimulation applications, but current applications are typically dependent on physiological loading. This is not always practical, as the individual may be non-weight bearing. To increase the effectiveness of these materials for clinical applications the use of ultrasound loading was investigated. Piezoelectric composite specimens (N=12) were manufactured using three PZT discs, wired with the intent to be connected in parallel, encapsulated with medical grade epoxy. The effect of ultrasound intensity (0.1, 0.5, and 1.0 W/cm<sup>2</sup>), compliant layer thickness (0.0 mm and 0.8 mm), and ultrasound application angle (0°, 45°, and 90°) on power generation was investigated for all specimens. Increased ultrasound intensity resulted in larger power production for all specimens. The 0.8 mm thickness group produced more power than the 0.0 mm group at an application angle of 0°, but this trend was reversed at angles of 45° and 90°. Lastly, the power output of all specimens decreased significantly in the 45° and 90° conditions compared to 0°. This study shows that ultrasound is a viable option for stimulating PZT composites intended for power generating applications where physiological loading isn't feasible.

### 3.2 Introduction

Each year there are over a million fractures that occur in the United States and approximately 5-10% of those fractures will result in a nonunion [2, 3]. When a bone breaks, whether it is a thick crack or complete break, it is referred to as a fracture and often is the result of an overload in functional capacity, trauma, or disease [4]. Depending on severity, some form of medical aid is often required, ranging from a splint to an intramedullary nail, but typically the fractured bone will fuse naturally. If a fracture fails to fuse in an appropriate amount of time it is classified as a non-union and may progress into pseudarthrosis, also known as false joint [5]. Nonunion is most common amongst tobacco users, diabetic, and elderly populations but can also be the result of an infection or severe break [6]. The natural bone remodeling process of individuals in these populations is impaired, inhibiting proper fusion of the bone. Individuals who develop a nonunion may suffer from an increased number of surgeries, limited use, pain, and swelling as well as increased costs, and inability to work [7].



Currently there are several adjunct therapies available for bone stimulation, ranging from extracorporeal shockwaves, ultrasound waves, and electrical stimulation [8]. The two most common bone stimulators on the market use Low Intensity Pulse Ultrasound (LIPU) or Direct Current (DC) electrical stimulation. Externally applied LIPU uses low intensity, high frequency, pulsed sound waves to interact with the fracture site. It is believed that the mechanical loads applied through ultrasound increase vascularization as well as stimulate osteocytes and osteoblasts, necessary for bone growth [9]. Although well known, the use of LIPU is not a universally accepted practice for fracture healing. DC stimulation creates an electrical potential using surgically implanted electrodes, driven by a battery pack, to apply a direct current to the fracture site. Research has shown a relationship between osteogenesis and DC stimulation when the cathode is placed near the fracture [10, 11]. These results are believed to be attributed to the natural piezoelectric property of bone [12, 13]. When a mechanical strain is applied to bone, a resultant electrical potential has been observed. This is commonly known as the piezoelectric effect. Although DC stimulation has shown positive results, it is not practical for everyday use due to the need for a battery pack and removal surgery. Therefore, there is a need for a technique that can electrically stimulate bone without batteries or secondary surgeries.

In recent years there has been an increasing trend in the use of piezoelectric materials for energy harvesting and power generation applications. Piezoelectric power generators are advantageous because they do not rely on batteries, which have limited lifespans, and typically do not require a removal surgery [14]. These materials have the ability to capture mechanical energy and convert it into a usable electrical charge. Several studies have been conducted using piezoelectric materials, in various configurations, to investigate their effectiveness for power generation and to enhance bone growth. Cochran et al. incorporated monolithic piezoelectric materials into an internal fixation device and showed that voltages in the range known to stimulate osteogenesis could be generated under physiological (walking) and external (ultrasound) loading conditions [15]. A study by Goetzinger et al. developed a spinal fusion implant by stacking multiple layers of macro fiber piezoelectric composite material [16]. This implant was later incorporated into a spinal fusion implant, used in a pilot ovine study, to generate power under a mechanical load delivering DC stimulation to an electrode placed near the fusion site [17]. Friis et al. showed that levels of DC stimulation sufficient to enhance bone growth were generated from this implant [16, 17]. These studies indicate there is a large potential for the use of piezoelectric materials in bone stimulation applications.

Piezoelectric materials have shown to be effective self-powering generators, but due to their poor source characteristics they are difficult to develop. Without modification, piezoelectric materials are known for their high voltage, low current, high impedance, and low power outputs [18]. Platt et al. investigated the effect of size and shape of piezoelectric elements on power generation. Results showed power generation was the same for both monolithic and stacked configurations, but stacked generators decreased the resistive load, decreased output voltage, and increased effective capacitance [18]. This same trend was observed in a more recent study by Goetzinger et al., who found that a significant decrease in load resistance occurred as the number of layers, within a composite stack, increased [16]. The addition of compliant layers, to a composite stack, was shown to result in an increased power generation by Krech et al. Compliant layer adaptive composite stacks (CLACS) incorporated an epoxy layer, of uniform thickness, between each piezoelectric disc. The amplification in power was attributed to the positive strain observed, as a result of compliant layers, increasing the piezoelectric effect produced [19]. These studies show that piezoelectric materials are a more viable option for various power generating applications when appropriately modified.

Much of the previous work involving piezoelectric materials in bone stimulation applications relied upon physiological loading, such as walking, to activate the piezoelectric material/implant. If an individual is classified as non-weight bearing, then physiological loading is not possible, and the piezoelectric material must be activated through another form of loading. This limitation is encountered quite frequently, as many long bone fractures require complete immobilization of the fractured bone. By developing a technique for loading the piezoelectric material, without relying on physiologically loading the injured area, the beneficial effects of bone stimulation through piezoelectric materials can be applied to a much larger number of injuries.

Therapeutic ultrasound is readily accessible, safe for medical applications, and has shown the ability to mechanically load structures within the body. Mechanical loading, along with other physiological interactions, are made possible through the propagation of high frequency (>20 kHz) sound waves in tissue. Depending on the intended application, parameters such as frequency, intensity, and application angle should be considered. Frequency (Hz) of ultrasound quantifies the number of sound waves emitted per second, is inversely related to wavelength, and is often correlated with penetration depth. Intensity (W/cm<sup>2</sup>) describes the power delivered in relation to the area across which it is distributed; therefore, the level of intensity directly effects the amount of

energy transfer. Lastly, application angle has been shown to have a significant effect on the amount of energy transferred from ultrasound, commonly seen in echo strength and temperature increases [20, 21].

The use of piezoelectric materials has a promising future in bone stimulation applications, but one major down side is that in many instances physiological loading is the primary mode of activation. It is not always practical to assume that the fracture site can be physiologically loaded. This points to the need for alternative modes of loading, such as ultrasound. The purpose of this study was to investigate the efficacy of ultrasound stimulation on piezoelectric composites used in power generation applications. Investigating the effects of ultrasound intensity, compliant layer thickness (CLACS), and application angle on power generation was the main goal. It was hypothesized that: (1) an increase in power generation would be observed with higher levels of ultrasound intensity, (2) increased power generation would be observed in the larger compliant layer group across all conditions, and (3) the highest power generation would be observed in the 0° testing condition when compared to alternate applications angles. Additional measurements of individual piezoelectric discs were collected, differing from the above measures which were collected for the complete stack. This information was used to further understand the contribution and effectiveness of each disc to aid in future design decisions. It was hypothesized that the discs further from the ultrasound transducer would produce less voltage.

### 3.3 Methods

#### 3.3.1 Composite Material Identification

Commercially available modified Navy Type I, PZT-4 Lead Zirconate Titanate (SM111), through thickness poled (3<sup>rd</sup>-axis) discs were used in this study (STEMiNC, Doral, FL). This material was selected for its high coupling coefficient ( $k_t = 0.45$ ) when compared to other forms of PZT material. Poling and electroding were completed under controlled conditions by the manufacturer. Positive and negative electrodes are located on the top and bottom faces of the disc, respectively. A two-component room temperature cure medical grade epoxy (EPO-TEK® 301, Epoxy Technology, Billerica, MA) was used to encapsulate PZT, forming the composite structure.

#### 3.3.2 Specimen Fabrication

Two groups of CLACS specimens were manufactured ( $n=6$ ,  $N=12$ ) with varying compliant layer thicknesses (0.0 mm, 0.8 mm  $\pm$  0.02 mm) [19]. Compliant layer thickness was determined based on an aspect ratio of PZT disc thickness. Specimens were fabricated with three 10 x 0.4 mm PZT discs encapsulated in medical grade epoxy, maintaining a constant volume of PZT as well as top, bottom, and side encapsulation thickness of 2 mm.

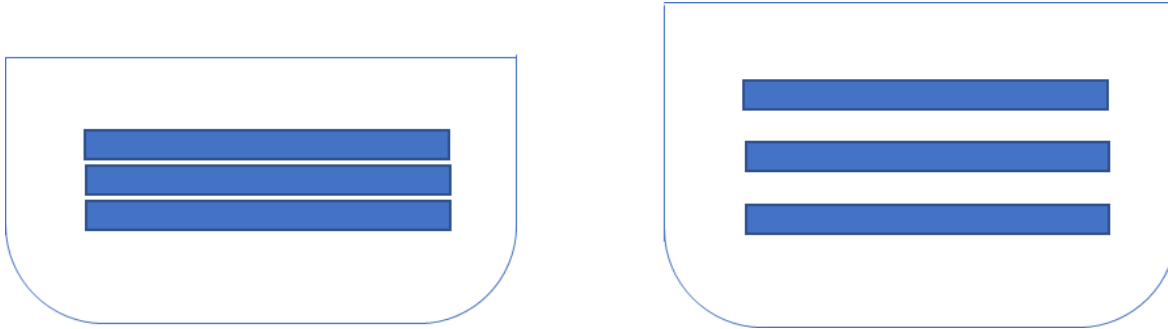


**FIGURE 9: ENCAPSULATION DESIGN SCHEMATIC FOR 0.0 MM (LEFT) AND 0.8 MM (RIGHT) COMPLIANT LAYER THICKNESSES**

Encapsulation design, shown in Figure 9, was developed to maintain a consistent distance traveled, through epoxy, of the ultrasound wave for all testing conditions. PZT discs were individually wired using conductive epoxy (EPO-TEK® H20E, Epoxy Technology, Billerica, MA) to adhere thin copper foil strips to the top and bottom of each disc. Once cured, the discs were stacked mechanically in series using an accordion style orientation, while maintaining a parallel electrical configuration of the stack [19]. Poling direction was verified prior to stacking to ensure appropriate separation of positive and negative electrodes. These wiring and assembly methods allowed for testing as a complete stack and investigation of individual disc output. In the 0.0 mm compliant layer group, a minimal amount of epoxy was used to adhere discs together and prevent shorting. The 0.8 mm compliant layer group used a minimal amount of epoxy to adhere pre-cured epoxy slices between each disc to create CLACS. After the stack is cured, a 2 mm precured slice of epoxy was adhered to the top and bottom of each specimen and allow time to cure. Then complete encapsulation was preformed to fully enclose the specimen, maintaining a constant shape and height, while also creating a 2 mm side epoxy thickness. Wires were soldered to copper strips at a temperature of 250°C, post encapsulation, to lengthen electrical leads for testing purposes. To ensure shorting did not occur during testing, the exposed copper strip and soldered connection were insulated using heat shrink and liquid electrical tape, as well as an external painted coat of medical grade epoxy to add structural integrity to the wires. Electrical connectivity, impedance, and capacitance values were measured for each disc and as a stack before and after ultrasound testing.

Stacking methods were performed in multiple steps to maintain uniform encapsulation dimensions and ensure that each disc was level, centered, and to eliminate the risk of shorting.

### 3.3.3 Ultrasound Testing

An Intellect Transport 2-Channel Electrotherapy (Chattanooga Group, Texas) machine with a 5 cm<sup>2</sup> transducer was used to mechanically load specimens. For all testing conditions the ultrasound setting was selected and set to a 1 MHz frequency and continuous duty cycle. Voltage measurements were acquired using an InfiniVision DSO-X 2012A 100 MHz Oscilloscope (Keysight Technologies, California). Specimens were encapsulated in gelatin with a 20 mm distance from the ultrasound transducer. Individual containers were developed, using plastic containers or plexiglass walls, to house encapsulated specimens with a thin layer of plastic film where the transducer would be applied. These containers are shown in Figure 10.

Specimens were first tested as a stack, measuring the voltage output with varying intensity (0.1 W/cm<sup>2</sup>, 0.5 W/cm<sup>2</sup>, 1 W/cm<sup>2</sup>), application angle (0°, 45°, 90°), and resistances. Loading conditions were selected to best characterize clinical standards and applications, as well as future implant design. To best characterize the performance of each stack, voltages were measured across a shunting resistance sweep (2.7 Ω – 800 Ω), this information will be utilized for future circuit design. In order to reduced thermal and pyroelectric effects from occurring, ultrasound was administered for 15 seconds on and then 15 seconds off during all testing conditions. This also allowed the researcher to capture steady state conditions by initiating data collection after the ultrasound had been administered for 10 seconds. Once the resistance sweep had been completed, to reduce over stimulation and skewed results, specimens remained untested for the same duration that testing had required prior to beginning the next testing cycle. Upon completion of stack testing, specimens were left in place and individual disc voltage outputs were measured under the same testing conditions to understand individual disc contributions. This testing was done immediately after, in order to ensure there was no variation in transducer location, application angle, and encapsulation.

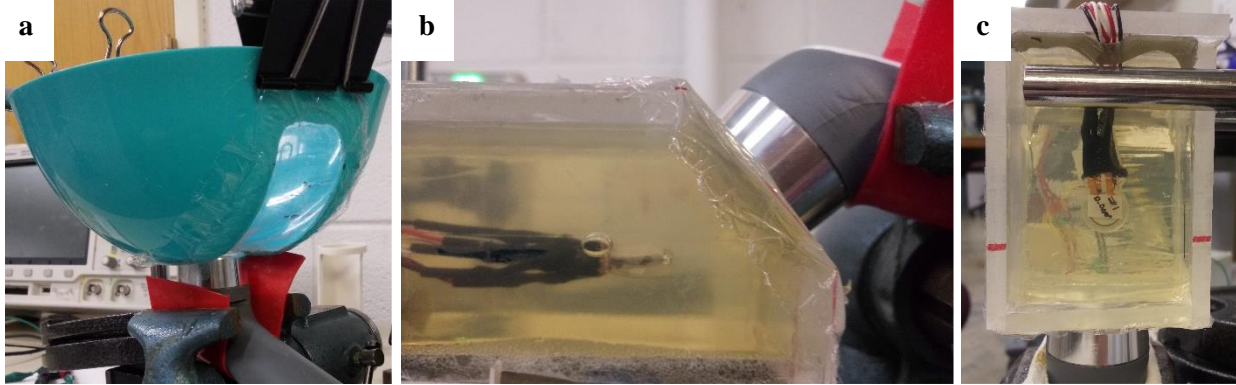


**FIGURE 10: APPLICATION ANGLE VARIATIONS A) 0 DEGREES, B) 45 DEGREES, C) 90 DEGREES**

### 3.3.4 Data and Statistical Analysis

Voltage data for each testing condition was exported from the oscilloscope as comma separate values file (.CSV) for data analysis. A MATLAB (MathWorks, Natick, MA) code was developed to import, filter, and analyze data. A 5<sup>th</sup> order low pass Butterworth filter with a cutoff frequency of 1.2 MHz was used to filter raw voltage data prior to data analysis. Filtered voltage was used in data analysis to obtain the root mean squared (RMS) voltage (Equation 2), and average maximum power (Equation 3) at each resistance. Upon completion of data analysis, a one-way analysis of variance (ANOVA) was used to determine if there were statistically significant differences in power production between compliant layer thickness, intensity, and application angle for all stacked specimen data. A Tukey Kramer post hoc analysis was used to determine significance between groups ( $\alpha = 0.05$ ). Prior to any statistical analysis, the log transformation of data was performed to satisfy normality and homogeneity of variance assumptions.

$$V_{RMS} = \frac{V_{OUT}}{\sqrt{2}} \quad (2)$$

**EQUATION 2: RMS VOLTAGE**

$$P = \frac{V_{RMS}^2}{R} \quad (3)$$

**EQUATION 3: POWER CALCULATION**

### 3.4 Results

A total of twelve CLACS specimens (n=6 for each group) were tested using ultrasound as the mode of mechanical loading. Voltage measurements, for all testing conditions, were measured across a shunting resistance

sweep ( $2.7 \Omega - 800 \Omega$ ) in order to best characterize power output. One 0.8 mm specimen was omitted from all data analysis due to a large decrease in capacitance measurements, indicating that multiple discs had likely been damaged or their piezoelectric properties were altered. Therefore, the 0.0 mm group results included six specimens and the 0.8 mm group results included five specimens.

### 3.4.1 Complete Stacks

#### 3.4.1.1 *Effect of Ultrasound Intensity*

Figure 11 shows average power generated by the specimens at each resistance for each ultrasound intensity. The highest power generation was observed for an ultrasound intensity of  $1.0 \text{ W/cm}^2$  for all testing conditions. In the 0.0 mm thickness groups, a significant difference was seen between the  $0.1 \text{ W/cm}^2$  and  $0.5 \text{ W/cm}^2$  conditions, and the  $0.1 \text{ W/cm}^2$  and  $1.0 \text{ W/cm}^2$  conditions. There was no significant difference in power generation between the  $0.5 \text{ W/cm}^2$  and  $1.0 \text{ W/cm}^2$  conditions. This trend was seen across all three angles of application.

Analyzing the 0.8 mm thickness groups, a statistical significance was observed between the  $0.1 \text{ W/cm}^2$  and  $1.0 \text{ W/cm}^2$  conditions. No significance was seen between  $0.1 \text{ W/cm}^2$  and  $0.5 \text{ W/cm}^2$ , or the  $0.5 \text{ W/cm}^2$  and  $1.0 \text{ W/cm}^2$  conditions. Peak average power output occurred at the same resistance ( $30 \Omega$ ) for all conditions other than 0.8 mm,  $1.0 \text{ W/cm}^2$ ,  $45^\circ$  and 0.8 mm,  $0.1 \text{ W/cm}^2$ ,  $90^\circ$ . For these two conditions, peak power occurred at the next resistance value ( $50 \Omega$ ).

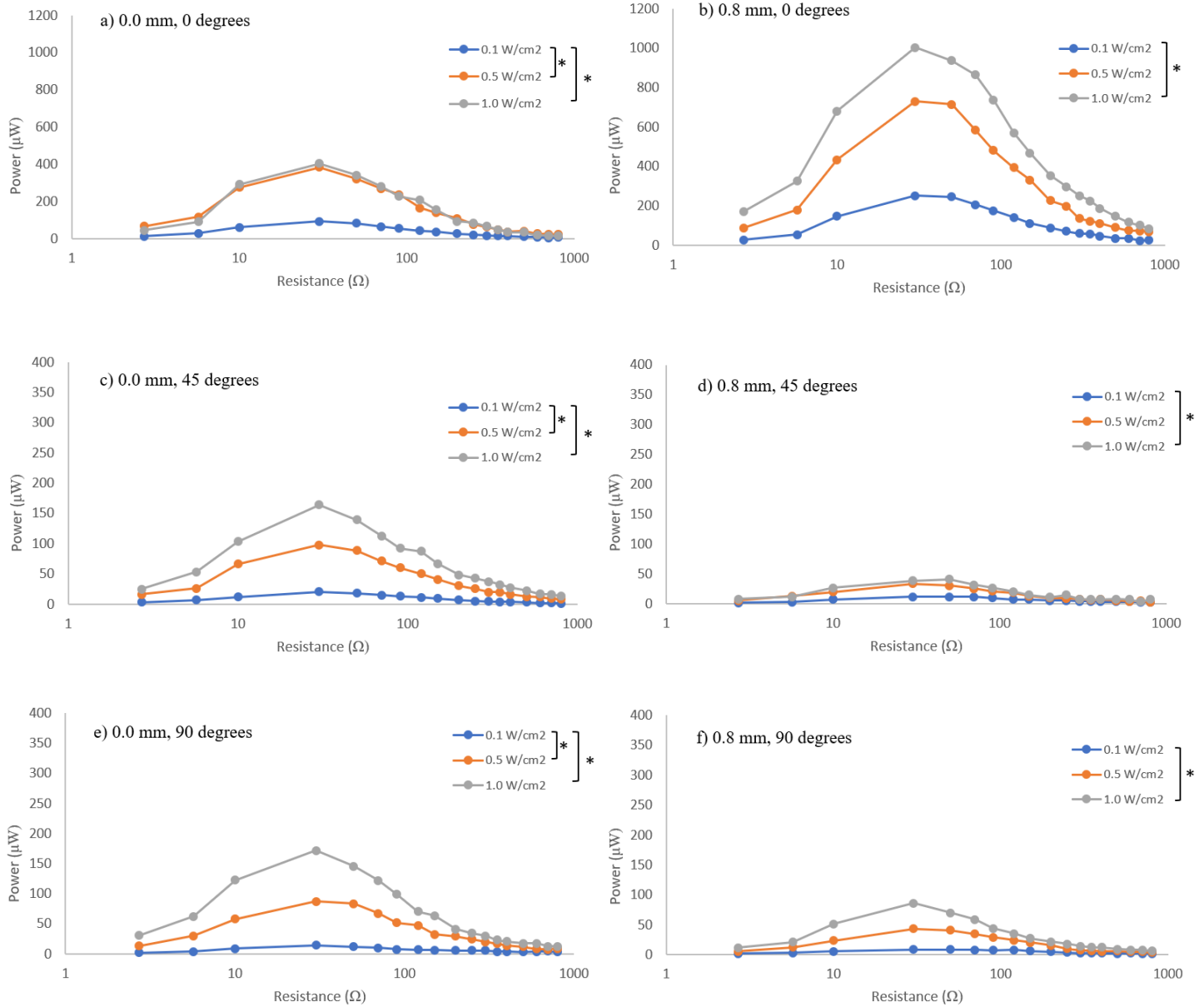


**FIGURE 11: AVERAGE POWER ACROSS THE RESISTANCE SWEEP FOR VARYING ULTRASOUND INTENSITIES. COMPLIANT LAYER THICKNESS AND APPLICATION ANGLE OF: A) 0.0 MM & 0°, B) 0.8 MM & 0°, C) 0.0 MM & 45°, D) 0.8 MM & 45°, E) 0.0 MM & 90°, F) 0.8 MM & 90°.**  
 [\* INDICATES SIGNIFICANCE WITH ALPHA=0.05]

### 3.4.1.2 Effect of CLACS

The average maximum power for each condition is represented in Table 2. In the 0° condition, the 0.8 mm specimens produced a higher power output. The increase in power was statistically significant in the 0.1 W/cm<sup>2</sup> and 1.0 W/cm<sup>2</sup> conditions. For the 45° and 90° conditions, the opposite trend was observed, with 0.0 mm specimens



producing a higher power output. In the 45° condition, at ultrasound intensities of 0.5 W/cm<sup>2</sup> and 1.0 W/cm<sup>2</sup>, a significant difference was observed. No significant differences were observed in the 90° conditions.

**TABLE 2: MAXIMUM POWER OUTPUT FOR 0.0 MM AND 0.8 MM COMPLIANT LAYER THICKNESSES**  
[\* INDICATES SIGNIFICANCE WITH ALPHA=0.05]

Ultrasound Intensity	Compliant Layer Thickness	Maximum Power Output (µW)						
		0 Degrees		45 Degrees		90 Degrees		
		mean	st dev	mean	st dev	mean	st dev	
0.1 W/cm <sup>2</sup>	0.0 mm	95	± 21	*	21	± 7	15	± 9
	0.8 mm	260	± 142		12	± 9	10	± 7
0.5 W/cm <sup>2</sup>	0.0 mm	385	± 121		98	± 51	90	± 65
	0.8 mm	757	± 555		36	± 25	45	± 23
1.0 W/cm <sup>2</sup>	0.0 mm	418	± 98	*	165	± 85	172	± 133
	0.8 mm	1078	± 459		46	± 21	86	± 58

### 3.4.1.3 Effect of Angle

From visual inspection of Figure 12, the power production considerably decreased for angles varying from 0°. The average maximum power was not significantly different between application angles of 45° and 90°. Results depicted in Figure 12 represent average maximum power for an ultrasound intensity of 0.5 W/cm<sup>2</sup>. The same results were observed for all ultrasound intensities. The average maximum power for all 0.0 mm specimens decreased by 75% and 77% from 0° to 45° and 0° to 90°, respectively. A larger decrease was seen amongst the 0.8 mm specimens, with decreases of 95% and 94%.

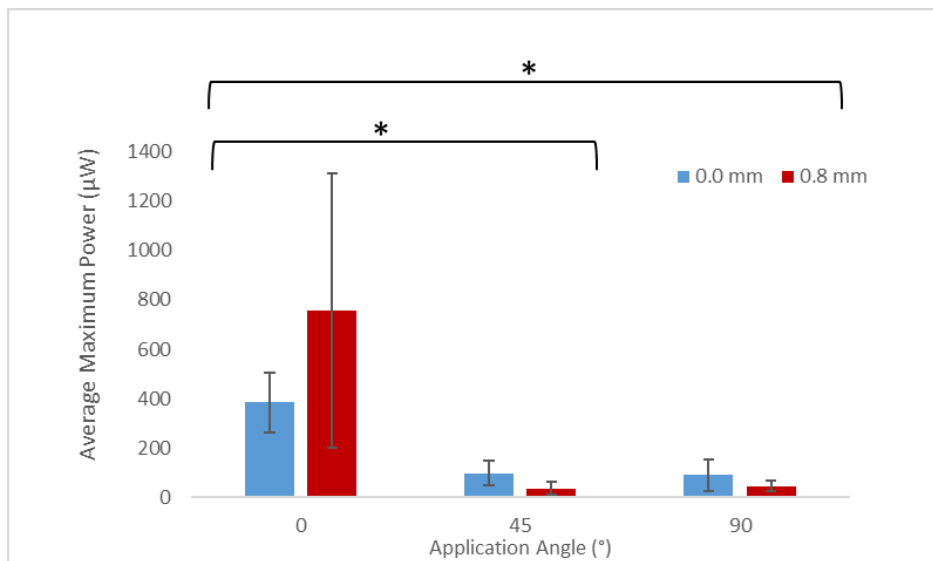


**FIGURE 12: AVERAGE MAXIMUM POWER VERSUS APPLICATION ANGLE (INTENSITY = 0.5 W/CM<sup>2</sup>)**  
[\* INDICATES SIGNIFICANCE WITH ALPHA=0.05]

### 3.4.2 Individual Disc Contribution

Figure 13 represents individual disc voltage outputs at 0° across varied ultrasound intensities. These measures were taken at 0° anticipating maximum output would occur at this angle, as it is the ideal loading orientation for this material. This information was used to create better understanding of individual disc contribution. In the 0.0 mm thickness group, the closest and furthest discs from the ultrasound transducer showed the highest voltage output but there was no significant difference between any discs at all intensities. For the 0.8 mm thickness group, the disc output voltage showed a decrease as the distance increased from the ultrasound transducer. A significant decrease was observed between discs 1 and 3 at all intensities, and between discs 2 and 3 at 0.1 and 0.5 W/cm<sup>2</sup> intensities.

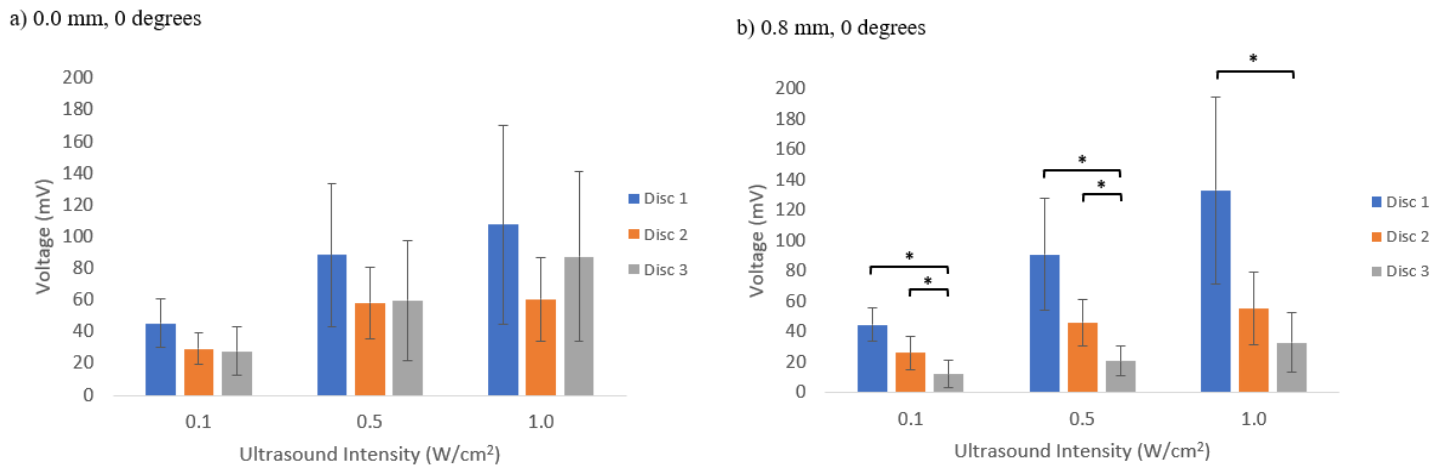


**FIGURE 13: CONTRIBUTIONS OF INDIVIDUAL DISC VOLTAGES TESTED AT 0 DEGREES WITH A COMPLIANT LAYER THICKNESS OF: A) 0.0 MM AND B) 0.8 MM [\* INDICATES SIGNIFICANCE WITH ALPHA=0.05]**

### 3.5 Discussion

The current study was designed to investigate the efficacy of using therapeutic ultrasound to stimulate PZT composites for power generating applications. This was completed by measuring the effects of ultrasound intensity, compliant layer thickness, and application angle on power generation. Ultrasound intensity values were selected to minimize potential thermal effects, while staying within the range considered to be safe for diagnostic imaging and/or therapeutic ultrasound uses. Previous literature has shown an increase in power generation for composites using CLACS under a cyclic compressive load designed to simulate the loading conditions of human motion. This

may not be applicable in all situations; therefore, the use of ultrasound was investigated to see if similar results could be achieved. Lastly, three application angles were chosen to best evaluate a range used in a clinical setting.

For therapeutic applications an increase in ultrasound intensity often results in a greater tissue response. An example of this is the use of low intensity ultrasound to accelerate soft tissue healing, by improving blood flow, and the use of high intensity ultrasound to break up kidney stones [9]. The idea that a higher intensity would elicit a greater response was exploited in this study, as it was hypothesized that a greater power generation would occur when higher intensity ultrasound was used, across all testing conditions. Based on the results represented in Figure 11, the original hypothesis was supported, but not all results showed a significant difference in power generation when varying ultrasound intensity. Although an increase in power output is desirable, the increase in applied ultrasound may not significantly increase power production. For example, in the 0.0 mm thickness group there was no significance between the 0.5 W/cm<sup>2</sup> and 1.0 W/cm<sup>2</sup> intensities, and in the 0.8 mm thickness group there was no significance between 0.1 W/cm<sup>2</sup> and 0.5 W/cm<sup>2</sup> as well as 0.5 W/cm<sup>2</sup> and 1.0 W/cm<sup>2</sup> intensities. This was attributed to the resonance frequency of the material. PZT material, found inside of each test specimen, functions most optimally when it reaches its resonance frequency, at this point the material is believed to be vibrating most readily [22]. It is believed that as intensity increases the material is approaching its resonance frequency. If the PZT discs inside of the specimens reach their resonance frequency, any changes beyond that point will not be as dramatic. As ultrasound intensity is increased, the chance of causing thermal effects is also increased [23]. Therefore, it is vital to find the most optimal intensity for power generation that does not result in harmful thermal effects.

The results of this study were similar to the findings of Krech et al. for testing performed in the same axial direction of PZT disc poling (0°). Testing in this direction showed an increase in power generation for 0.8 mm specimens across all intensities, but this trend was reversed for off axis testing orientations (45°, 90°). For testing performed off axis, in the 45° and 90° orientation, increased power generation was observed for 0.0 mm specimens across all intensities. These trends can be observed through visual inspection of Table 2, but there is only a significant difference in power generation for intensities of 0.1 W/cm<sup>2</sup> and 1.0 W/cm<sup>2</sup> in the 0° orientation, and 0.5 W/cm<sup>2</sup> and 1.0 W/cm<sup>2</sup> conditions in the 45° orientation.

It is the displacement of the dipoles within piezoelectric materials that results in the electrical charge generated for energy harvesting and power generation applications [14]. This displacement is the result of an applied

mechanical strain or vibration. Previous researchers have attributed the increased power production, observed in CLACS, to an increased positive strain of the in-plane direction. For CLACS, this strain is a result of the compressive load applied in the axial direction of poling and has an additive effect on power output. Although ultrasound is a form of mechanical loading, the effects vary from typical compressive loading techniques. The mechanical effects observed in ultrasound are commonly measured with pressure changes rather than deformation [24]. As the high frequency ultrasound wave travels through a medium, particles rapidly vibrate, creating cyclic compressive and rarefactive patterns [25]. Therefore, ultrasound mechanical loading, as utilized in this study, does not generate the same levels of deformation seen in the Krech et al. study. This may be why increased power production was only seen from the 0.8 mm CLACS specimen in the 0° orientation. These results did not agree with the original hypothesis that a larger compliant layer thickness would result in an increased power generation in all testing conditions.

Ultrasound therapy, in a clinical setting, is usually applied in a continuous motion to treat a larger area, as well as to reduce thermal effects at higher intensities and duty cycles. Meanwhile, piezoelectric materials are anisotropic, meaning they are directionally dependent. In order to appropriately stimulate a clinical application of ultrasound, testing was performed at various angles. It was hypothesized that maximum power generation for each thickness group would be observed at the 0° condition. This was anticipated because PZT materials often respond most efficiently when loaded along the same axis as their poling direction. This hypothesis was validated by the results seen in Figure 12. A significant difference in power generation was seen between 0° and 45° applications, and 0° and 90° applications, across all conditions. A decrease in power generation was observed for both the 0.0 mm and 0.8 mm thickness groups when varying angle, but the magnitude of that change was higher in the 0.8 mm group. Compliant layers increase the amount of strain observed by the PZT discs between each layer, increasing the overall piezoelectric output. It is believed that this is only true when loading along the direction of poling. If off axis loading occurs, the material's deformation is less uniform, creating a negative, dampening, effect in the compliant layer region. This results in the effectiveness of the PZT being decreased. When comparing the power production at the 45° and 90° condition no significant difference was observed, this trend was also seen in the percent decrease calculations when comparing to 0°. Once loading is applied off axis, a decrease in power generation is to be expected but once a certain threshold is exceeded the outputs do not significantly differ from one another, as seen when comparing the 45° and 90° conditions.

For future implant design PZT specimens will be fully wired as a stack, but for this study specimens were fabricated to allow for individual disc measurements to be recorded. The idea behind this fabrication method was to quantify individual disc contributions. Ultrasound waves naturally attenuate the further they travel through a medium, but increased attenuation is often observed when a boundary of different impedance is encountered, most commonly seen between soft tissue and bone. In this study the ultrasound wave must travel through gelatin, representing soft tissue, epoxy, and PZT; all of which vary in impedance. Therefore, it was hypothesized that discs further from the ultrasound transducer would produce less voltage. For the purpose of discussing these results, discs will be referred to by number 1, 2, and 3 with 1 being closest to the ultrasound transducer and 3 being the furthest. Only the 0.8 mm thickness group supported this hypothesis, as seen in Figure 13, significant decreases were observed between discs 1 and 3 at all intensities, as well as between discs 2 and 3 at intensities of 0.1 and 0.5 W/cm<sup>2</sup>. The 0.0 mm thickness group showed the lowest output in disc 2, meaning the highest outputs were exhibited in discs 1 and 3, respectively, although none of these differences were significant. The addition of compliant layers between discs has shown an overall increase in stack output but the exact thickness that most optimally satisfies this observation has yet to be identified. Therefore, it is possible that the top and bottom encapsulation of the 0.0 mm thickness specimens are acting as a compliant layer resulting in increased activity in neighboring discs.

### 3.6 Conclusion

This study investigated a novel method for stimulating piezoelectric composite materials used in power generation applications. The ability to generate power using ultrasound was shown in all specimens tested in this study. A significant difference in power production was shown with an increase in ultrasound intensity, compliant layer thickness, and variation of application angle. Parameters chosen for this study are most commonly used in therapeutic ultrasound applications, and they all showed considerable power production. Having the ability to use ultrasound, as a means of loading, can make piezoelectric composites an even more desirable material for power generating modalities. In bone stimulating applications it introduces a treatment possibility for non-weight bearing individuals but could also be used as an enhancement therapy to physiological loading.

Future research directions should include the design of an implant that integrates a piezoelectric composite and will optimally perform under ultrasound loading. Ideally, the implant would be designed in order to perform optimally under both ultrasound and physiological loading. This study intended to strictly investigate the efficacy of using ultrasound to simulate piezoelectric composites, and several design considerations would need to be addressed

when translating this research to a medical device. Through further research, the most optimal ultrasound parameters for stimulating piezoelectric composites will be achieved and maximal power output will be produced.

### 3.7 Acknowledgements

The authors would like to thank Kyle Coates, Craig Cunningham, Tori Drapel, and Zach Pessia at the University of Kansas, along with Dr. Terence McIff from the University of Kansas Medical Center, for their advice and assistance on this project. They also would like to thank University of Kansas Medical Center - Physical Therapy Department for providing the ultrasound unit necessary to complete this research

### 3.8 Funding Data

This work was supported by the KU RESEARCH GO Grant ([Grant Number here](#)).

### 3.9 Nomenclature

PZT – Lead Zirconate Titanate  
CLACS – Compliant Layer Adaptive Stacks  
LIPU – Low Intensity Pulsed Ultrasound  
DC – Direct Current  
CSV – Comma-Separated Values  
ANOVA – Analysis of Variance  
RMS – Root Mean Square

### 3.10 References

1. Marina Del Ray Hospital. *What are the most common orthopedic surgeries?* 2019; Available from: <https://www.marinahospital.com/faq/what-are-the-most-common-orthopedic-surgeries>.
2. Zura, R., et al., *Epidemiology of Fracture Nonunion in 18 Human Bones*. JAMA Surg, 2016. **151**(11): p. e162775.
3. Cleveland Clinic. *Bone Fractures*. 2017; Available from: <https://my.clevelandclinic.org/health/diseases/15241-bone-fractures>.
4. American Academy of Orthopedic Surgeons. *Fractures (Broken Bones)*. Diseases & Conditions 2012; Available from: <https://orthoinfo.aaos.org/en/diseases--conditions/fractures-broken-bones/>.
5. Martin, R.B., D.B. Burr, and N.A. Sharkey, *Skeletal tissue mechanics*. 1998, New York: Springer. xiv, 392 p.
6. American Academy of Orthopedic Surgeons. *Nonunions*. Diseases & Conditions 2014; Available from: <https://orthoinfo.aaos.org/en/diseases--conditions/nonunions/>.
7. Tay, W.H., et al., *Health outcomes of delayed union and nonunion of femoral and tibial shaft fractures*. Injury, 2014. **45**(10): p. 1653-8.
8. Wienke, J. and P. Payton, *Bone Stimulation For Nonunions: What The Evidence Reveals*. Podiatry Today, 2011. **24**(9): p. 52-57.
9. Miller, D.L., et al., *Overview of therapeutic ultrasound applications and safety considerations*. J Ultrasound Med, 2012. **31**(4): p. 623-34.

10. Aaron, R.K., D.M. Ciombor, and B.J. Simon, *Treatment of nonunions with electric and electromagnetic fields*. Clin Orthop Relat Res, 2004(419): p. 21-9.
11. Rubinacci, A., et al., *Changes in bioelectric potentials on bone associated with direct current stimulation of osteogenesis*. J Orthop Res, 1988. **6**(3): p. 335-45.
12. Yasuda, I., *Piezoelectricity of Living Bone*. Journal of Kyoto Prefectural University of Medicine, 1953. **53**(325).
13. Fukada, E. and I. Yasuda, *On the Piezoelectric Effect of Bone*. Journal of the Physical Society of Japan, 1957. **12**(10): p. 5.
14. Li, H., C. Tian, and Z.D. Deng, *Energy harvesting from low frequency applications using piezoelectric materials*. Applied Physics Reviews, 2014. **1**(4): p. 041301.
15. Cochran, G.V., et al., *Piezoelectric internal fixation devices: a new approach to electrical augmentation of osteogenesis*. J Orthop Res, 1985. **3**(4): p. 508-13.
16. Goetzinger, N.C., et al., *Composite piezoelectric spinal fusion implant: Effects of stacked generators*. J Biomed Mater Res B Appl Biomater, 2016. **104**(1): p. 158-64.
17. Friis, E.A., S.N. Galvis, and P.M. Arnold, *DC Stimulation for Spinal Fusion with a Piezoelectric Composite Material Interbody Implant: An Ovine Pilot Study*. 2015.
18. Platt, S.R., S. Farritor, and H. Haider, *On low-frequency electric power generation with PZT ceramics*. IEEE/ASME Transactions on Mechatronics, 2005. **10**(2): p. 240-252.
19. Krech, E.D., et al., *Effect of compliant layers within piezoelectric composites on power generation providing electrical stimulation in low frequency applications*. J Mech Behav Biomed Mater, 2018. **88**: p. 340-345.
20. Kimura, I.F., et al., *Effects of two ultrasound devices and angles of application on the temperature of tissue phantom*. J Orthop Sports Phys Ther, 1998. **27**(1): p. 27-31.
21. Bahner, D.P., et al., *Language of Transducer Manipulation: Codifying Terms for Effective Teaching*. J Ultrasound Med, 2016. **35**(1): p. 183-8.
22. APC International, L., *Piezoelectric Ceramics: Principles and Applications*. 2011: APC International.
23. Draper, D.O., J.C. Castel, and D. Castel, *Rate of temperature increase in human muscle during 1 MHz and 3 MHz continuous ultrasound*. J Orthop Sports Phys Ther, 1995. **22**(4): p. 142-50.
24. Sen, T., O. Tufekcioglu, and Y. Koza, *Mechanical index*. Anatol J Cardiol, 2015. **15**(4): p. 334-6.
25. Lake, D., *Chapter 4: Therapeutic Ultrasound*, in *Modalities for Therapeutic Intervention*. 2012, F.A. Davis Co.: Philadelphia. p. xxix, 460 p.

## Chapter 4: Conclusions and Future Work

### 4.1 Conclusions

The goal of this study was to determine the efficacy of using ultrasound to stimulate piezoelectric composites for power generating applications. Overall, power was generated by piezoelectric composites when loaded with ultrasound, but the amount produced was dependent upon the testing conditions. Ultrasound intensity, compliant layer thickness, and application angle were the primary testing conditions investigated. It was shown that an increase in intensity resulted in an increase in power generation across all testing conditions. Increased compliant layer thickness (0.8 mm) showed increased power generation when loaded in line with the PZT poling direction, but the reverse was observed for off axis loading conditions with increased power seen in the specimens with no compliant layers (0.0 mm). Power generation decreased in all testing conditions when the applied angle was varied from the PZT poling direction. A larger percent decrease was observed in specimens with increased compliant layer thickness (0.8 mm). While investigating individual disc voltage output, it was found that the voltage produced decreased as the distance from the transducer increased in the 0.8 mm group. On the other hand, the highest voltage output was seen in the closest and furthest discs, for the 0.0 mm group.

### 4.2 Limitations

Several limitations to this study were that each of the PZT discs was electrically soldered by the researcher, discs were all wired individually, and specimen placement may have varied slightly between tests. Although the manufacturer's directions for soldering were strictly followed, it is possible that material characteristics were altered due to the heat transferred by the soldering iron. Capacitance measurements were recorded for all discs, due to its relationship to power, to indicate variations and possible damage prior to testing. Many of the measurements recorded in this study were obtained for the complete PZT stack, but each disc within the stack was wired separately and connected externally. It is possibly that this could have resulted in unknown electrical variations. Lastly, it is important to note that naturally an ultrasound beam is nonhomogeneous, as defined by the beam non-uniformity ratio (BNR).



This describes the ratio of the highest intensity within the beam field to the average intensity indicated by the unit. Due to this inherent characteristic of ultrasound, any difference in placement could result in variation amongst the energy transferred to the PZT specimens. Ultrasound transducer and specimen placement were kept as uniform as possible, but a small degree of possible variation was unavoidable.

#### 4.3 Future Work

Future research directions should include improving the design of an implant that integrates a piezoelectric composite and optimizing an ultrasound transducer for this application. Ideally, the implant would be designed for non-weight bearing applications, such as long bone fractures, that utilize an intramedullary nail or bone plate, but the implant should be designed such that it performs optimally under both ultrasound and physiological loading conditions. This study intended to strictly investigate the efficacy of using ultrasound to simulate piezoelectric composites, and several design considerations would need to be addressed when translating this research to a medical device.

Through further research, the most optimal ultrasound parameters and transducer design for stimulating piezoelectric composites will be achieved and maximal power output will be produced. Increased coupling could be achieved by designing an ultrasound transducer to match the curvature of physiological structures. This increase in coupling would then result in an increase in signal transmission and energy transfer to the implant. Additionally, being able to more accurately match multiple layers of varying impedance should be incorporated in transducer design in order to best match the intended application.

Finally, the use of ultrasound to stimulate piezoelectric composites should be investigated in other applications that would benefit from electrical stimulation. Neurological applications would be an example of this by providing a means to electrically stimulate the brain without requiring the use of a battery pack. Soft tissue stimulating applications could also benefit from the use of this technology due to their anatomical location and simplicity of applying ultrasound to the injury location.

## Appendix A: Supplementary Figures

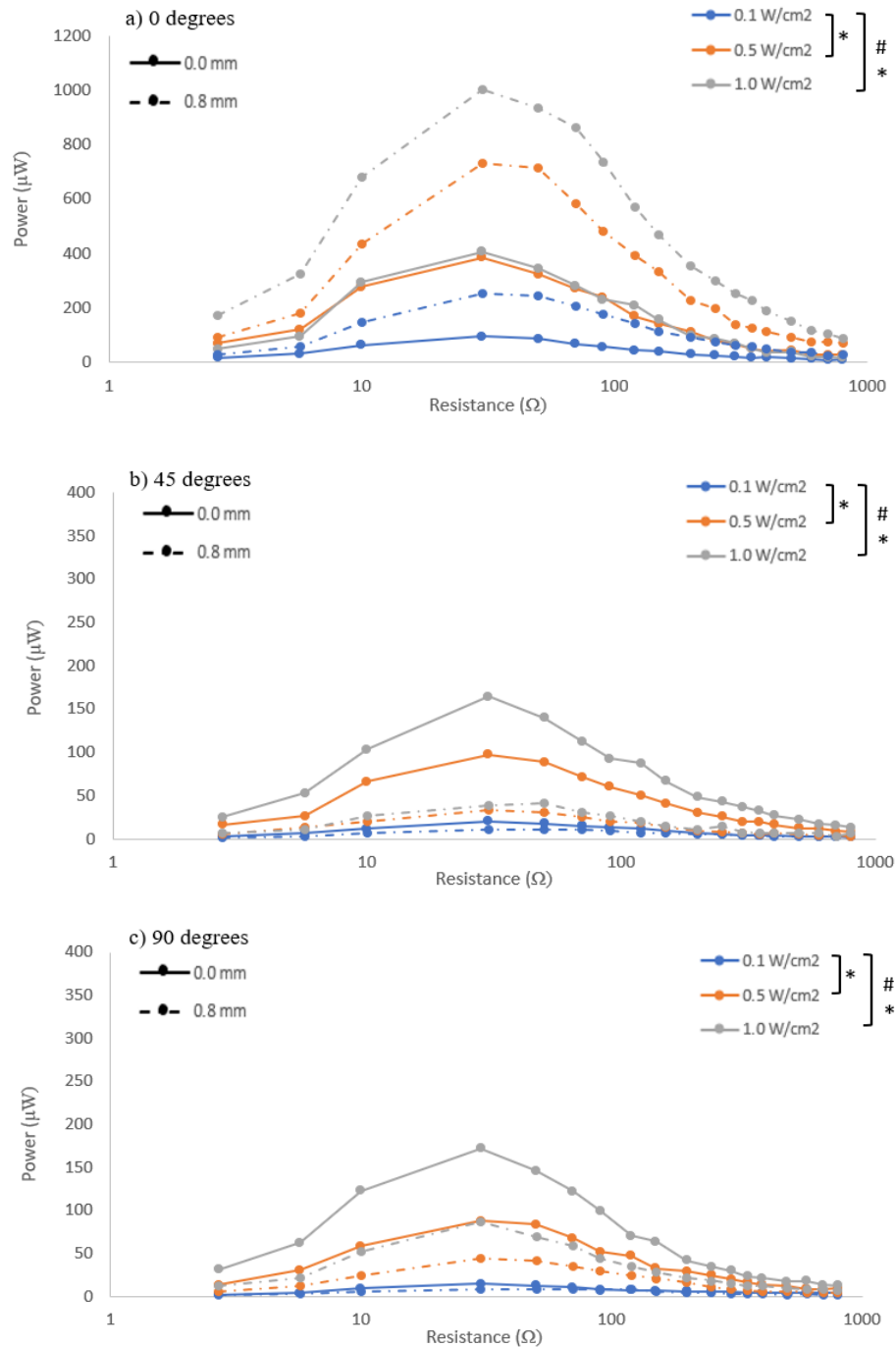


**FIGURE 14: AVERAGE POWER ACROSS THE RESISTANCE SWEEP FOR VARYING ULTRASOUND INTENSITIES. COMPLIANT LAYER THICKNESS AND APPLICATION ANGLE OF: A) 0.0 MM & 0.8 MM 0°, B) 0.0 MM & 0.8 MM 45°, C) 0.0 MM & 0.8 MM 90°.**

[\* INDICATES SIGNIFICANCE AMONGST 0.0 MM GROUP WITH ALPHA=0.05,  
# INDICATES SIGNIFICANCE AMONGST 0.8 MM GROUP WITH ALPHA=0.05]

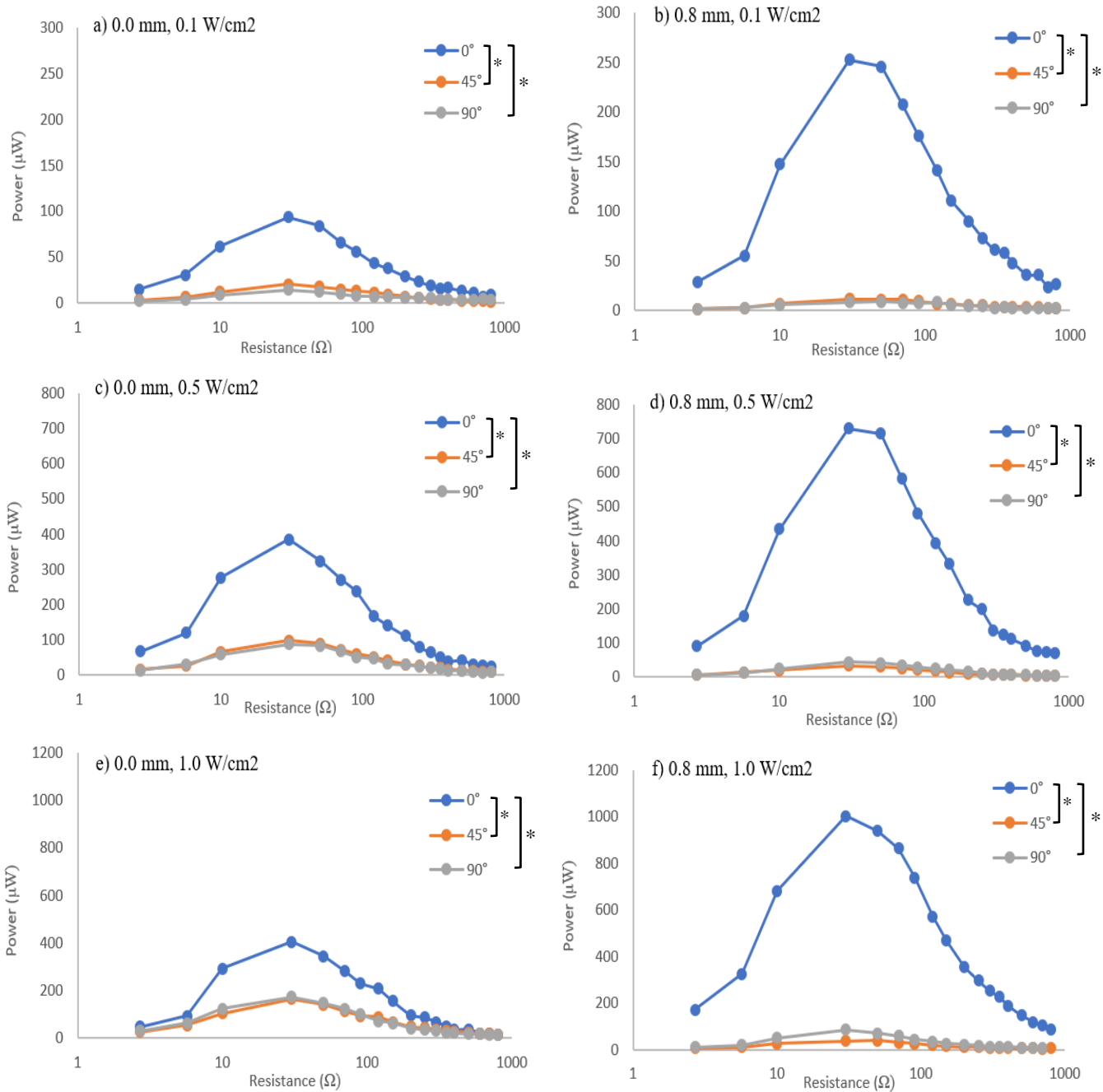


**FIGURE 15: AVERAGE POWER ACROSS THE RESISTANCE SWEEP FOR VARYING APPLICATION ANGLES. COMPLIANT LAYER THICKNESS AND INTENSITY OF: A) 0.0 MM & 0.1 W/CM<sup>2</sup>, B) 0.8 MM & 0.1 W/CM<sup>2</sup>, C) 0.0 MM & 0.5 W/CM<sup>2</sup>, D) 0.8 MM & 0.5 W/CM<sup>2</sup>, E) 0.0 MM & 1.0 W/CM<sup>2</sup>, F) 0.8 MM & 1.0 W/CM<sup>2</sup>.**

[\* INDICATES SIGNIFICANCE, FOR BOTH GROUPS, WITH ALPHA=0.05]

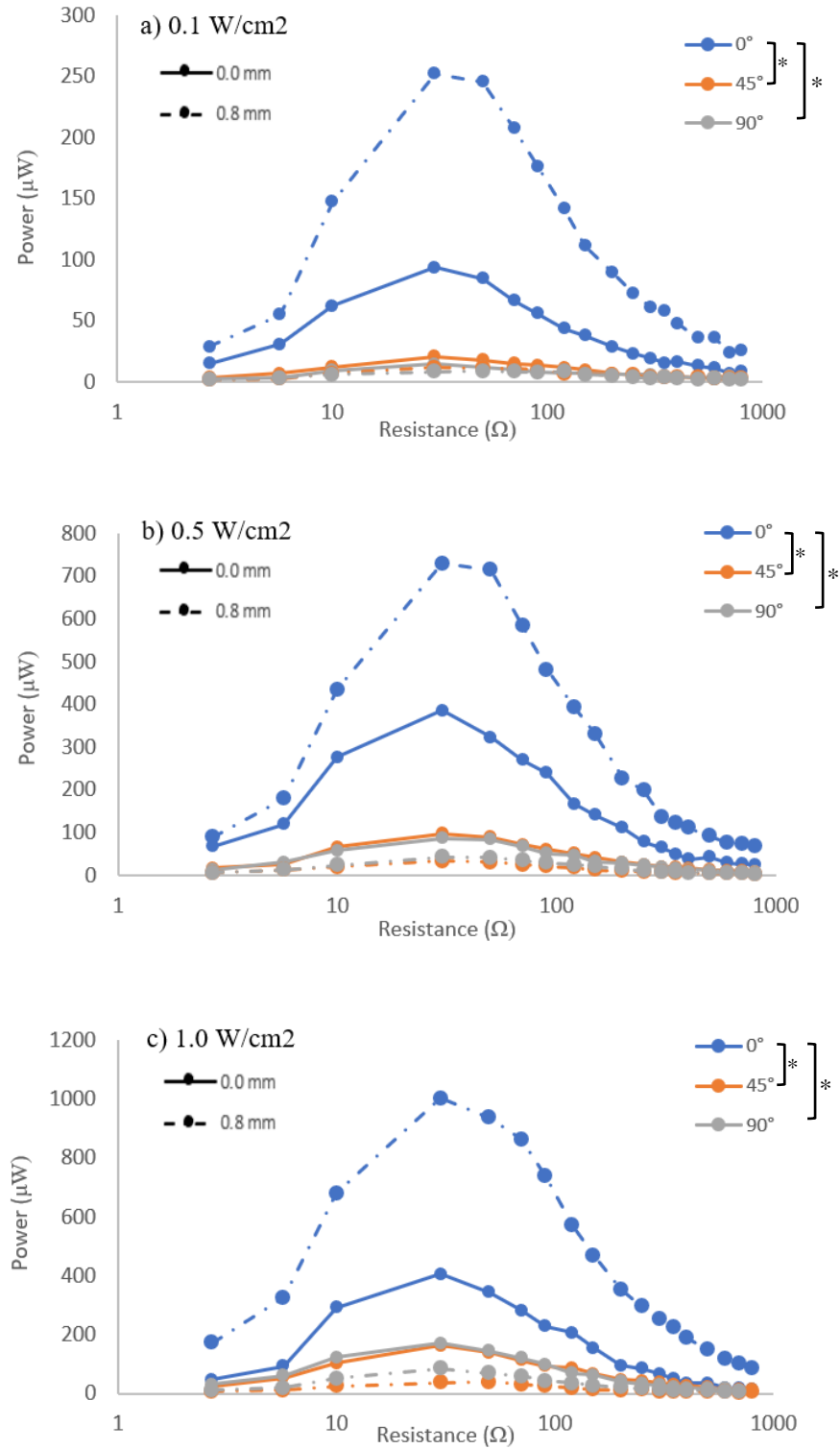


**FIGURE 16: AVERAGE POWER ACROSS THE RESISTANCE SWEEP FOR VARYING APPLICATION ANGLE. COMPLIANT LAYER THICKNESS AND INTENSITY OF: A) 0.0 MM & 0.8 MM, 0.1 W/CM<sup>2</sup>, B) 0.0 MM & 0.8 MM, 0.5 W/CM<sup>2</sup>, C) 0.0 MM & 0.8 MM, 1.0 W/CM<sup>2</sup>. [\* INDICATES SIGNIFICANCE, FOR BOTH GROUPS, WITH ALPHA=0.05]**

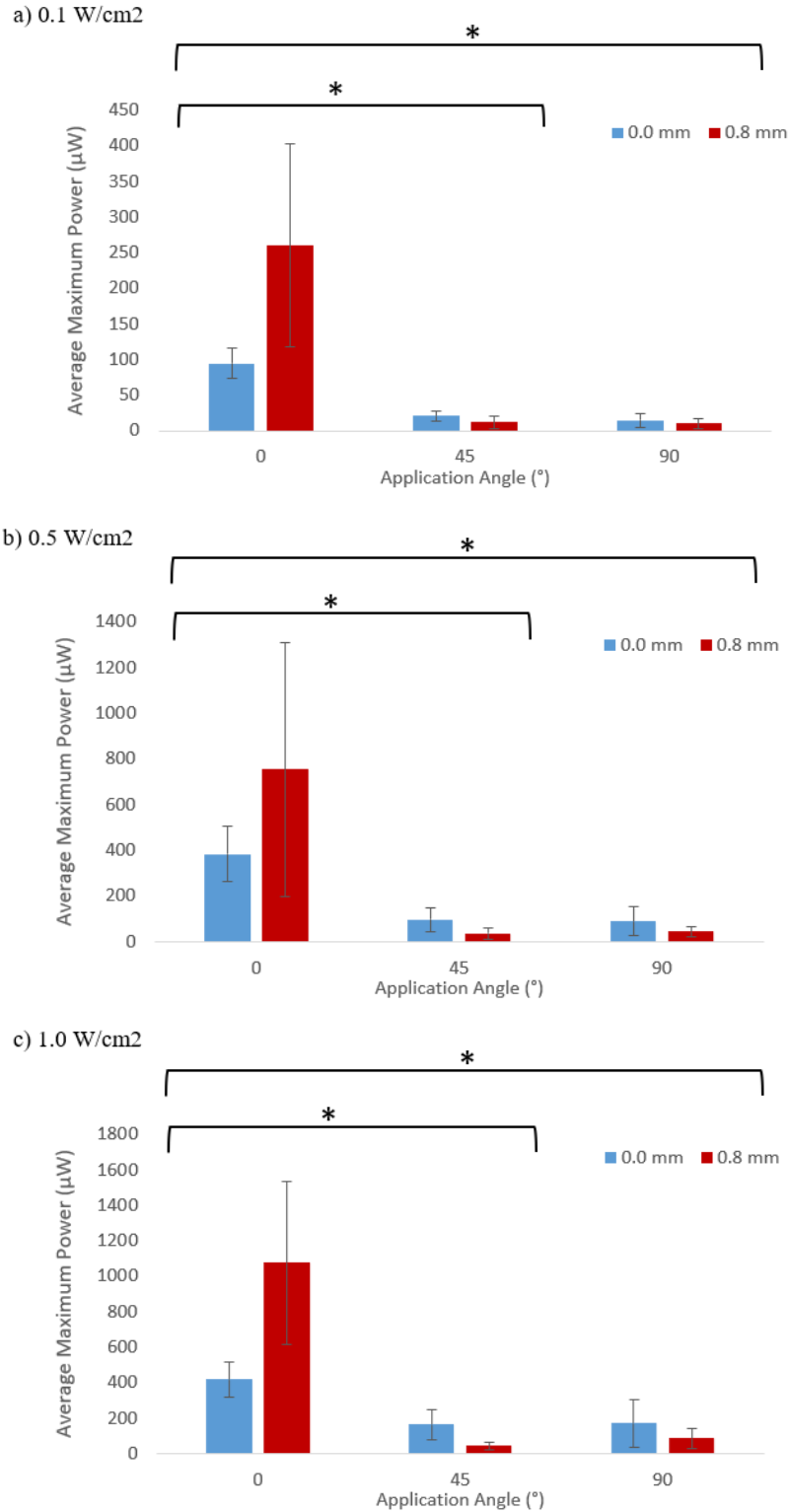


**FIGURE 17: AVERAGE MAXIMUM POWER VERSUS APPLICATION ANGLE COMPLIANT LAYER THICKNESS AND INTENSITY OF: A) 0.0 MM & 0.8 MM 0.1 W/CM<sup>2</sup>, B) 0.0 MM & 0.8 MM 0.5 W/CM<sup>2</sup>, C) 0.0 MM & 0.8 MM 1.0 W/CM<sup>2</sup>**

**[\* INDICATES SIGNIFICANCE, FOR BOTH GROUPS, WITH ALPHA=0.05]**

## Appendix B: Detailed Methods

### Fabrication

Below are detailed steps involved in manufacturing the test specimens used in this study. When handling bare PZT discs, always wear gloves and use caution so the silver electrode surface is not scratched, and discs are not at risk of being damaged.

#### *Verification Step - Poling Direction*

1. Many premanufactured disc's poling directions are marked, but it is important to verify poling direction of all discs before fabrication.
2. Each disc is marked with an engraved plus sign on the positive pole. First, place the negative side down onto a piece of aluminum sheet metal, ensuring that something is placed between the aluminum sheet and the table, for insulation.
3. Using a multimeter set to read DC voltage, gently touch the positive, red, lead to the top of the disc and the negative, black, lead to the aluminum sheet. Be sure not to scratch the PZT disc.
4. Exhale a quick puff of air aimed at the disc, then check the voltage output on the multimeter. If the output voltage is positive, then the poling direction as marked is correct. If the opposite occurs and a negative voltage is observed, then the poling direction is reversed. If this occurs, mark the correct positive side of the disc with a red dot.
5. Repeat this process for all discs prior to electrical connection.

#### *Electrical Connection*

1. Using copper foil, cut two 43 mm x 2 mm (length x width) copper strips per disc. Be careful not to wrinkle or bend the strips.
2. Lay three PZT discs on a rectangular piece of Delrin with their positive side facing upward. (Note: This is to make one specimen, multiple groups can be completed at one time.)
3. Apply conductive epoxy (EPO-TEK® H20E) to the top of each disc, away from the plus sign so it remains visible. The epoxy area should be slightly smaller than the width of the copper strip, in order to decrease overflow of epoxy when the copper foil is pressed in place. (Note: overflow will increase the difficulty of stacking the discs as they will want to tilt and not stay level.)
4. Using tweezers, hold the PZT disc in place as the copper foil is placed on the conductive epoxy. There should be some adherence, but the copper foil should not be flush to the disc yet. Each disc should have its own individual copper strip adhered to each side.
5. Let go of the disc and use the same tweezers to lightly push down on the copper foil along the face of the disc. It should now be flush.
6. Place a circular slice of silicon on top of the disc and copper foil to completely cover each disc.
7. Once this has been completed for every disc in the batch, ensure all discs are in a straight line and gently place a long piece of steel on top of them. Be sure that the silicon is between the disc and metal, and that all discs are weighted by the steel.
8. Cure in the oven at 130°C for 30 minutes.
9. After the elapsed time, pull the discs out but do not remove the weight. Set aside and allow time to cool (~1 hour). (Note: if they are not cooled properly the copper foil will not adhere to the disc.)
10. After cooling, use tweezers to carefully remove circular silicon cut outs. If the conductive epoxy overflowed it may stick to the silicon and separate the copper strip from the disc. Therefore, it is important to remove the discs slowly in order to minimize the chance of this occurring.
11. Verify the copper strip is fully adhered to the disc.
12. Flip the discs over so the negative side is now facing upward. Repeat the above steps, but place the copper foil on the opposite side of the disc. Placing the copper foil on the opposite side ensures that the copper strips do not touch and create an electrical short.

13. Once copper foil has been adhered to both the positive and negative sides of the PZT disc, cut a small amount off the copper strip attached to the negative side. This will help identify positive and negative connections later in the fabrication process to decrease errors.
14. Move all discs to a silicon mat. Verify electrical connection using a voltmeter set to read resistance.
15. Place the positive, red, lead to the positive copper strip and the negative, black, lead to the negative copper strip. The output should read over-load (O.L).
16. To verify copper strips are connected to each disc, place one lead of the multimeter on the copper strip and the other on the face of the PZT disc (of the same pole, i.e. positive strip, positive face). The multimeter should output a low resistance.
17. Repeat for all discs to verify they are all electrically connected and not shorting.

### *Stacking*

These two methods should coincide with one another to reduced material waste as there are multiple steps and the minimum batch size for epoxy is much larger then what is needed to create each specimen.

#### **0.0 mm Specimen**

1. Make a batch of medical grade epoxy (EPO-TEK® 301).
2. Arrange three discs in a row with alternating poles facing upward (ex: positive, negative, positive). This is how they will be stacked, keeping the positives and negatives together.
3. For the 0.0 mm specimen, paint a small coat of epoxy on the upward face of disc 1 and 2, in the above orientation. Be sure to cover the entire face of the disc and keep the epoxy coat as level as possible, this is to prevent electrical shorting.
4. Set these aside as they require 24 hours room temperature cure, then 2 hours 65°F post cure in the oven.
5. Allow the excess epoxy to sit for 2 hours, increasing in viscosity and becoming “goopy”.
6. Dab a small amount of goopy epoxy to the upward face of disc 3 and place the pre-cured top encapsulation epoxy slice on top (2 mm thickness). Once complete, set aside and allow time to cure as described in step 4.
7. Once cured, verify electrical connection. If the discs are not shorting, mix a new batch of epoxy and allow time to get goopy.
8. Dab a small amount of goopy epoxy to the face of discs 1 and 2, then stack these two discs, keeping them as aligned and level as possible. Using the orientation mentioned in step 2, keep the positives and negative together and ensure top encapsulation is on top of the stack.
9. All copper strips should be on the same side, for later encapsulation, therefore caution must be taken to ensure they are not touching. A small dab of epoxy can be added between strips if touching is occurring (note: this must be done before the stack is completely cured).
10. Set aside to cure as described in step 4.
11. Once the stack is cured, verify electrical connection. If the discs are not shorting, mix a new batch of epoxy and allow time to get goopy.
12. Dab a small amount on a precured bottom encapsulation with a 2mm thickness and filleted edges. Place the stack on the bottom encapsulation, ensuring it is as centered and flat as possible.
13. Set aside to cure as described in step 4.
14. Once cured, verify electrical connection. If the discs are not shorting, mix a new batch of epoxy and place the stack into a silicon mold. The copper strips should be facing upward and protruding out of the mold, arrange copper strips so they are not touching. Once the epoxy is cured, the copper strips within the encapsulation are difficult to move; therefore, it is important to ensure they are not touching prior to curing.
15. Slowly pour epoxy into the silicon mold, periodically lightly squeezing the mold to allow air bubbles to move up to the top for removal. The top and bottom encapsulation previously added ensure that the PZT stack will not tip or float, keeping the discs centered.
16. Allow 24 hours to cure at room temperature, then removed the fully encapsulated specimen from the mold and place in a 65°F oven for post cure.
17. Once fully cured, check electrical connections once again.

## 0.8 mm Specimen

1. Make a batch of medical grade epoxy (EPO-TEK® 301).
2. Arrange three discs in a row with alternating poles facing upward (ex: positive, negative, positive). This is how they will be stacked, keeping the positives and negatives together.
3. For the 0.8 mm specimen, dab a small amount of goopy epoxy to the upward face, using the orientation described in step 2. Place pre-cured compliant layer slices on top of discs 1 and 2 and place a precured top encapsulation on top of disc 3. This should create a 0.8 mm compliant layer between each disc and a 2 mm top encapsulation.
4. Set these aside as they require 24 hours room temperature cure, then 2 hours 65°F post cure in the oven.
5. Once cured, verify electrical connection. If the discs are not shorting, then mix a new batch of epoxy and allow time to get goopy.
6. Dab a small amount of goopy epoxy to the face of disc 1 and 2 then stack discs, keeping them as aligned and level as possible. Using the orientation mentioned in step 2, keep the positives and negative together, ensure the compliant layer is between discs, and the top encapsulation is on top of the stack.
7. All copper strips should be on the same side, for later encapsulation, therefore caution must be taken to ensure they are not touching. A small dab of epoxy can be added between strips if touching is occurring (note: this must be done before the stack is completely cured).
8. Set aside to cure as described in step 4.
9. Once the stack is cured verify electrical connection. If the discs are not shorting mix a new batch of epoxy and allow time to get goopy.
10. Dab a small amount on a precured bottom encapsulation with a 2 mm thickness and filleted edges. Place the stack on the bottom encapsulation ensuring it is as centered and flat as possible.
11. Set aside to cure as described in step 4.
12. Once cured, verify electrical connection. If the discs are not shorting, mix a new batch of epoxy and place the stack into a silicon mold. The copper strips should be facing upward and protruding out of the mold, arrange copper strips so they are not touching. Once the epoxy is cured, the copper strips within the encapsulation are difficult to move; therefore, it is important to ensure they are not touching.
13. Slowly pour epoxy into the silicon mold, periodically lightly squeezing the mold to allow air bubble to move up to the top for removal. The top and bottom encapsulation added previously ensures the PZT stack will not tip or float, keeping the discs centered.
14. Allow 24 hours to cure at room temperature, then removed the fully encapsulated specimen from the mold and place in a 65°F oven for post cure.
15. Once fully cured check electrical connection.

## *Wire Connection*

Once specimens are completely encapsulated, and electrical connection has been verified, insulated wires can be soldered to the copper strips to increase the length of the leads and insulate wires for testing purposes.

1. Clamp and secure the epoxy portion of the specimen using a Neiko Adjustable helping hand. Orient the specimen when soldering so the wires are flush with the table, this will make wire attachment easier.
2. Separate the positive and negative copper strips of each disc by carefully flipping them up or down. Only one set of copper strips, one positive and negative, should be flush on the table to decrease error.
3. Wires used were separated from 326-DTV Micro-Measurements 3 conductor cable.
4. Cut ~200 mm length wire and strip ~5mm of each end of the wire. Solder the exposed end of each wire at 250°C to the copper strip.
5. Tape was placed on each wire to indicate what disc it belongs to (green= disc 1, yellow=disc 2, and red=disc 3). Disc 1 correlates to the bottom disc which will be closest to the ultrasound transducer, and disc



3 is the top and furthest. Although wires can be visibly matched with their disc this allows for easy identification.

6. Once all wires are attached and labeled, all positives and negatives should be bundled and taped together for ease of testing.
7. Place heat shrink tubing around any exposed copper and soldered connections. Once in place, use a heat gun to shrink the tubing in place.
8. Apply liquid electrical tape around the edge between the epoxy encapsulation and wire connection to seal any gaps that may still be present. Only apply liquid tape near the wires and keep it away from the testing surface.
9. Apply any necessary additional coats every 10 minutes. Once completed, allow 24 hours to dry.
10. Make a batch of epoxy, painting it over the liquid tape and heat shrink insulation areas. Once cured, this will increase strength of the wires and decrease chance of exposure if bent.
11. Allow 24 hours room temperature cure and 2 hours 65°C post cure in the oven.
12. Once cured, verify electrical connection and record capacitance measurements of each disc and as a stack.

### Medical Grade Epoxy Mixture:

1. 4:1 mix ratio (Part A:B respectively).
2. Minimum Batch Size: 5g.
3. Do not use a container with any inside coating (this is an exothermic reaction and coatings can mix into the epoxy).
4. Once both parts are added, mix in a circular motion, alternating directions periodically until homogeneous (streaks in the mixture should no longer be visible).
5. Allow 5-10 minutes for the exothermic reaction to occur, mix once more, the use as necessary.

### Gelatin

1. A 500mL glass beaker was used for gelatin mixtures.
2. Fill the beaker with 237mL (~1 cup) of deionized water.
3. Place beaker on a hot plate set to 180°C and add three 0.25oz packets of gelatin to water. Add a stir bar to the beaker to mix contents. Allow 10 minutes to heat and mix.
4. Remove gelatin mixture and visually inspect the mixture verifying all gelatin powder has dissolved. Then remove from heat and allow 30 minutes to cool.
5. Once cooled, pour the gelatin mixture into the test containers filling only half (marked on each contain with a line).
6. Place in refrigerator and allow 1-2 hours to gel.
7. Once gelled, place the test specimen in the correct location so that it is 20 mm away from the ultrasound transducer (indicated by marks on test containers). Ensure that the side without wires is facing/closest to the side of the container where the transducer will sit (plastic film).
8. Wires will need to be taped to the wall of the container to hold specimen in place.
9. Pour a small gelatin layer into the container covering only half of the specimen. Allow 30 minutes in the refrigerator to gel. The test specimen will float when fully submerged; therefore, this section of gelatin holds the specimen in place, keeping it completely flat, which is imperative for testing.
10. Fill the rest of the container with gelatin to fully submerge the specimen and allow 1-2 hours to completely gel.
11. Once gelled, verify electrical connection and record capacitance measurements for each disc and as a stack.

### Ultrasound Testing

1. Place testing container in the proper orientation for the desired testing orientation (0°, 45°, 90°). Use clips to suspend containers for 0°, and 90° testing.

2. Clamp the ultrasound transducer into a swivel multiangle vise with the head facing upward for 0° and 90° testing, and downward for the 45° testing.
3. Apply a uniform layer of ultrasound gel (used for coupling) to the head of the transducer, then rotate the vise to position the transducer in the appropriate location. The ultrasound head should be flush with the plastic film of the testing container.
4. Once in place, do not move the transducer or container for the duration of the test.
5. Turn on the ultrasound unit and select the third option listed as ultrasound.
6. Set the frequency to 1 MHz, duty cycle to continuous, display W/cm<sup>2</sup>, intensity to 0.1 W/cm<sup>2</sup>, and warming to off.
7. Connect the test specimen, as a stack, to channel 1 of the oscilloscope. Using alligator clips, the positive lead of the test specimen should connect to the input of the RC box, the output of the RC box should go into the positive of the oscilloscope cable, and the negative lead of the specimen should connect to the negative of the oscilloscope cable.
8. Before testing begins turn on the oscilloscope and plug in a USB drive to save the data files.
9. Set the name according to thickness\_angle\_intensity\_specimen#\_resistance# (ex: 0t\_45d\_05w\_2\_01, indicating a 0mm thickness, 45° angle, 0.5 W/cm<sup>2</sup> intensity, specimen 2, and resistance value 1 in the sweep) file type to .CSV, data points to 2000, and scale to 2μs.
10. Begin testing by pressing start on the ultrasound unit.
11. After 10 seconds, save the waveform represented on the oscilloscope. It is important to wait 10 seconds before saving in order to allow steady state conditions to occur.
12. Pause the ultrasound unit after 15 seconds. Allow specimen to sit, with no ultrasound stimulation being applied, for 15 seconds. During this time, the resistance on the RC box must be changed to the next increment of the resistance sweep (2.7Ω-800Ω).
13. Repeat steps 11 & 12 until all resistances have been tested.
14. Once the resistance sweep has been completed, rename the data file, to represent the next test, and increase the intensity to 0.5 W/cm<sup>2</sup>.
15. Repeat steps 10, 11 and 12.
16. Once complete, rename the data file and increase the intensity to 1.0 W/cm<sup>2</sup>.
17. Repeat these steps for all testing conditions and specimens.
18. If testing the 0° testing condition, leave the testing container in place once all testing has been completed on the stack.
19. Reconnect wires to the RC box and oscilloscope so that individual disc wires are connected rather than the entire stack. This will have to be done one at a time, starting with disc 1, then moving to discs 2 and 3.
20. For individual disc testing, use the following naming convention:  
thickness\_angle\_intensity\_specimen#\_disc#\_resistance# (ex: 2t\_0d\_01w\_1\_d1\_05).
21. A smaller resistance sweep was used for individual discs (10Ω-250Ω). This ensures that the resistance at which max power was achieved for each stack was captured for each individual disc.
22. Repeat steps 5-15 for each test specimen using the resistance sweep described in step 20.
23. Once all testing is completed, verify electrical connection and record capacitance measurements for each disc and as a stack.

## Appendix C: Data Processing Code

### Main Stack Analysis MATLAB Code

```
% Main Analysis code written to analyze ultrasound-PZT stack data
% Written by Morghan Alters.
% Modified from code written by Ember Krech.
% Last update: 11/25/19

clear; clc; close all;

%% Input Parameters

frequency = 1e6; % Hz - ultrasound probe frequency

%This is the complete resistance sweep (# of resistors # range of resistors) -
Modify as necessary
resistance_sweep = [0 3 0 20 40 60 80 110 140 190 240 290 340 390 490 590 690
790];

%% Load Desired Data

count = 1; % figure counter
countresults = 1;
countall=1;

file_path = 'E:\Morghan\TEST\reorganized';

% Analysis
% Create a FOR loop to analyze CLACS of 0.0mm and 0.8mm
% "i" index , "n" name , "a" abbreviation
for ithickness = 1:2 % Run from 1:2
    if ithickness == 1
        nthickness = '0.0mm';
        athickness = '0t';
    else
        nthickness = '0.8mm';
        athickness = '2t';
    end

    %Create a FOR loop to analyze each angle of application
    for iangle = 1:3 % Run from 1:3
        if iangle == 1
            nangle = '0 degrees';
            aangle = '0d';
        elseif iangle == 2
            nangle = '45 degrees';
            aangle = '45d';
        else
            nangle = '90 degrees';
            aangle = '90d';
        end

        countsub = 1;
        %Create a FOR loop to analyze each ultrasound power intensity used
```

```

for ipower = 1:3      %Run from 1:3
    if ipower == 1
        npower = '0.1 W';
        apower = '01w';
    elseif ipower == 2
        npower = '0.5 W';
        apower = '05w';
    else
        npower = '1.0 W';
        apower = '1_w';
    end

    %Create a FOR loop to analyze each specimen
    for ispecimen = 1:6      % Run from 1:6
        nspecimen = ['Specimen ' int2str(ispecimen)];

        % Omit the 0.8mm thick, Specimen #3 from our data
        if ithickness==2 && ispecimen==3
            continue
        end

        for iResistor = 1:length(resistance_sweep)
            % resistance of the oscilloscope
            if iResistor ==1
                Rosc=2.7;
            elseif iResistor==2
                Rosc=2.7;
            else
                Rosc=10;
            end

            % Define and read the raw data file
            file_location = [file_path nthickness '\\' nangle '\\'
npower '\\' nspecimen '\\'];
            data_file = [athickness '_' aangle '_' apower '_'
int2str(ispecimen) '_' num2str(iResistor, '%.2d.csv')];
            input_name = [file_location data_file];
            data = dlmread(input_name, ',', 2, 0);           % read in
            oscilloscope data files

            % Define the output file
            specimen_name = [nthickness ' - ' nangle ' - ' npower ' -
' nspecimen];
            output_file = [file_location specimen_name];

            Rvar = resistance_sweep(iResistor);           % resistance
            value in ohms

            % Variable Identification
            time = data(:,1);                             % seconds
            voltage = data(:,2);                          % volts
            voltage = voltage-mean(voltage);              % center data
            around zero

            raw_voltage(:,iResistor)=voltage;             % all raw
            voltage data

```

```

% Calculate the sample frequency
deltaT = diff(time);           % sampling freq
DeltaT = mean(deltaT);        % Side note may
all be the same number
fs = 1 / DeltaT;

% FFT and power spectrum calculation
N=2048;                         % N points (2^n)
for the FFT

dt=1/fs;                         % time between
samples
range=(N/2);                     % range for the
spectral plot
f=fs*(0:range-1)/N;             % frequency axis
(note: starts at 0)

Y=fft(voltage);                 % FFT using 2000
data points
Pyy=Y.*conj(Y)/N;              % Calculate the
Power spectrum

% PLOT the power spectrum of each data series
% figure(1)
% subplot(2,1,1)
% plot(time,Y)
% title('FFT')
% xlabel('time (s)')
% ylabel('Amplitude (V)')
%
% hold on
%
% subplot(2,1,2)
% plot(f',Pyy(1:range))
% title('Power Spectrum');
% xlabel('Frequency (Hz)')
% ylabel('V^2')
%
% hold on

% Filter
fc = 1.2e6;                       %
cutoff frequency

[b,a] = butter(5,2*fc/fs);        %
(Nth order, cutoff frequency)how to determine cutoff freq
Vosc = filtfilt (b,a,voltage);

% Second FFT and power spectrum calculation AFTER lowpass
filter

% figure(2)
% Y=fft(Vosc);                     % FFT
using 2000 data points

```

```

Calculate the Power spectrum
%          Pyy=Y.*conj(Y)/N;
%
%          subplot(2,1,1)
%          plot(time,Y)
%          title('FFT')
%          xlabel('time (s)')
%          ylabel('Amplitude (V)')
%
%          hold on
%
%          subplot(2,1,2)
%          plot(f',Pyy(1:range))
%          title('Power Spectrum');
%          axis ([0 100 0 .005]);
%          xlabel('Frequency (Hz)')
%          ylabel('V^2')
%
%          hold on

% Variable calculations for voltage and power
Vosc = Vosc*(1/sqrt(2));
convert to RMS voltage
Vout = Vosc.*(1+(Rvar/Rosc));
% scale voltage by the applied resistance - find voltage produced by the
speciman
Vamp = (max(Vout) - (min(Vout)))/2;
peak-to-peak voltage (amplitude)
P = Vout.^2./(Rvar+Rosc);
instantaneous power
Pavg = trapz(time,P) * 1/(max(time) - min(time));
average power
Pmax = Vamp.^2./(Rvar+Rosc);
peak power per cycle
Pmaxu = Pmax*(10^6);
peak power in uW

%% Store data to output

rsweep(iResistor,1) = Rvar+Rosc;
output(iResistor,specimen) = Pmaxu;
output2(iResistor,1) = Pmaxu;

rsweeplog = log(rsweep);

all_resistances(iResistor,countall)=Pmaxu;

end

% Used when plotting the power curves
% rsweeplog2(:,1) = rsweeplog;
% rsweeplog2(:,2) = rsweeplog;
% rsweeplog2(:,3) = rsweeplog;

% Save all results for further analysis in SAS
% Uncomment these two lines and comment out step above (line
68)

```

```

        % that omits a specimen from the data if exporting to SAS
        [M, I]=max(output2);
        % all_results(countall,:) = [ithickness iangle ipower
ispecimen M I];

        countall = countall+1;
end

% Re-organize the output matrix to be nx5 for 0.8mm
if ithickness==1
else
    output2(:,1)=output(:,1);
    output2(:,2)=output(:,2);
    output2(:,3)=output(:,4);
    output2(:,4)=output(:,5);
    output2(:,5)=output(:,6);

%!!!!!!!!!!!!!!!!!!!!!!!!!!!!!!!!!!!!!!!!!!!!!!!!!!!!!!!!!!!!!!!!!!!!!!!!!!!!

%!!!!!!!!!!!!!!!!!!!!!!!!!!!!!!!!!!!!!!!!!!!!!!!!!!!!!!!!!!!!!!!!!!!!!!!!!!!!
!!!!!!!!!!!!!!!!!!!!

        % change to match number of specimens used
        output=output2;
end

outputavg(:, ipower)=mean(output,2);
outputstd(:, ipower)=std(output,0,2);

all_avgs(:, countresults) = outputavg(:, ipower);
all_stds(:, countresults) = outputstd(:, ipower);

[resultsavg(ipower, iangle), index]=max(mean(output,2));

stdev=std(output,0,2);
resultsstd(ipower, iangle)=stdev(index);

resultscv=resultsstd./resultsavg;

if ithickness ==1
    resultsavg1=resultsavg;
    resultsstd1=resultsstd;
    resultscv1=resultscv;
else
    resultsavg2=resultsavg;
    resultsstd2=resultsstd;
    resultscv2=resultscv;
end

% Plot the power curves for each specimen and averages
hold on

figure(count)

subplot(2,2, countsub)

plot(rsweeplog, output)

```

```

%
%         hold on
%         if countsub== 1
%             axis([0 7 0 500])
%         elseif countsub==2
%             axis([0 7 0 1500])
%         else
%             axis([0 7 0 2000])
%         end
%
%         xlabel('Resistance (ohms)')
%         ylabel('Power (microW)')
%         title(npower)
%         legend('1','2','3','4','5','6')
%
%
%         countsub=countsub+1;
%
%         if countsub==4
%             subplot(2,2,countsub)
%
%             hold on
%             if countsub== 4 && iangle== 1
%                 axis([0 7 0 2000])
%             elseif countsub== 4 && iangle== 2
%                 axis([0 7 0 1200])
%             else
%                 axis([0 7 0 400])
%             end
%
%             errorbar(rsweeplog2,outputavg,outputstd)
%             xlabel('Resistance (ohms)')
%             ylabel('Power (microW)')
%             title('Averages')
%             legend('0.1 W', '0.5 W', '1.0 W')
%         end
%
%         countresults = countresults + 1;
end
count = count+1;
end

end

%% Output to an excel sheet for later analysis

[max, max_avg_ind]=max(all_avgs);

% These two lines are commented out so that data is not over-written each
% time the code is executed

%
save('results.mat','rsweep','resultsavg1','resultsavg2','resultsstd1','result
sstd2','resultscv1','resultscv2','all_avgs','all_stds')
% save('input_discs.mat','max_avg_ind');

```



```

%% Save the "All Results" matrix for further analysis in SAS
% filename='all_results_stacks.xlsx';
% writematrix(all_results,filename,'Sheet',1,'Range','A1')

%%
disp('Done')

```

---

## Main Discs Analysis MATLAB Code

```

%% Main Analysis code written to analyze ultrasound-PZT individual disc data
% Written by Morghan Alters.
% Last update: 11/26/19

clear; clc; close all;

%% Input Parameters

load('input_discs.mat')

max_avg_ind=max_avg_ind-2; %remove the 2 resistances that are omitted in the
single disc sweep
index1=reshape(max_avg_ind(1:9),[3,3]); % rows are power, 1=0.1, 2=0.5, 3=1.0
index2=reshape(max_avg_ind(10:18),[3,3]); % columns are angle, 1=0d, 2=45d,
3=90d

% Removing the 90d trials, and rotating to match subplot layout
index1=index1(:,1:2)'; %rows are now angle of application, 1=0d, 2=45d
index2=index2(:,1:2)'; %columns are now power, 1=0.1, 2=0.5, 3=1.0

frequency = 1e6; % Hz - ultrasound probe frequency

%This is the complete resistance sweep (# of resistors # range of resistors) -
Modify as necessary
resistance_sweep = [0 20 40 60 80 110 140 190 240];

%% Load Desired Data
countresults = 1;

file_path = 'E:\Morghan\TEST\reorganized\';

% Analysis
% Create a FOR loop to analyze CLACS of 0.0mm and 0.8mm
% "i" index , "n" name , "a" abbreviation
for ithickness = 1:2 % Run from 1:2
    if ithickness == 1
        nthickness = '0.0mm';
        athickness = '0t';
    else
        nthickness = '0.8mm';
        athickness = '2t';
    end

    %Create a FOR loop to analyze each angle of application
    for iangle = 1:2 % Run from 1:2
        if iangle == 1
            nangle = '0 degrees';

```

```

        aangle = '0d';
    else
        nangle = '45 degrees';
        aangle = '45d';
    end

%Create a FOR loop to analyze each ultrasound power intensity used
for ipower = 1:3      %Run from 1:3
    if ipower == 1
        npower = '0.1 W';
        apower = '01w';
    elseif ipower == 2
        npower = '0.5 W';
        apower = '05w';
    else
        npower = '1.0 W';
        apower = '1_w';
    end

%Create a FOR loop to analyze each specimen
for ispecimen = 1:6      % Run from 1:6
    nspecimen = ['Specimen ' int2str(ispecimen)];

    % Omit the 0.8mm thick, Specimen #3 from our data
    if ithickness==2 && ispecimen==3
        continue
    end

%Create a For loop to analyze each individual disc
for idisc = 1:3
    ndisc = ['disc ' int2str(idisc)];
    adisc = ['d' int2str(idisc)];

    for iresistor = 1:length(resistance_sweep)
        % resistance of the oscilloscope
        Rosc=10;

        % Define and read the raw data file
        file_location = [file_path nthickness '\\' nangle '\\'
npower '\\' nspecimen '\\' ndisc '\\'];
        data_file = [athickness '_' aangle '_' apower '_'
int2str(ispecimen) '_' adisc '_' num2str(iresistor, '%.2d.csv')];
        input_name = [file_location data_file];
        data = dlmread(input_name, ',', 2, 0);          % read
in oscilloscope data files

        % Define the output file
        specimen_name = [nthickness ' - ' nangle ' - ' npower
' - ' nspecimen];
        output_file = [file_location specimen_name];

        Rvar = resistance_sweep(iresistor);          % resistance
value in ohms

        % Variable Identification
        time = data(:,1);                            % seconds

```

```

        voltage = data(:,2);           % volts
        voltage = voltage*1000;       % convert to
mV
        voltage = voltage-mean(voltage); % center data
around zero

        % Calculate the sample frequency
        deltaT = diff(time);         % sampling
freq
        DeltaT = mean(deltaT);       % Side note
may all be the same number
        fs = 1 / DeltaT;
        dt=1/fs;                     % time
between samples

        % Filter
        fc = 1.2e6;
% cutoff frequency
        [b,a] = butter(5,2*fc/fs);
% (Nth order, cutoff frequency)how to determine cutoff freq
        Vosc = filtfilt (b,a,voltage);

        % Variable calculations for voltage and power
        Vosc = Vosc*(1/sqrt(2));
% convert to RMS voltage
        Vout = Vosc.*(1+(Rvar/Rosc));
% scale voltage by the applied resistance - find voltage produced by the
speciman
        Vamp = (max(Vout) - (min(Vout)))/2;
% peak-to-peak voltage (amplitude)
        P = Vout.^2./(Rvar+Rosc);
% instantaneous power
        Pavg = trapz(time,P) * 1/(max(time) - min(time));
% average power
        Pmax = Vamp.^2./(Rvar+Rosc);
% peak power per cycle
        Pmaxu = Pmax*(10^6);
% peak power in uW

        %% Store data to output
        rsweep(iresistor,1) = Rvar+Rosc;
        output(iresistor,1) = Vamp;

    end

    if idisc==1
        output_d1(:,ispecimen)=output;
    elseif idisc==2
        output_d2(:,ispecimen)=output;
    else
        output_d3(:,ispecimen)=output;
    end

end

end

%Averages

```

```

d1_avg=mean(output_d1,2);
d2_avg=mean(output_d2,2);
d3_avg=mean(output_d3,2);
d_avg=[d1_avg, d2_avg, d3_avg];

%Standard Deviations
d1_std=std(output_d1,0,2);
d2_std=std(output_d2,0,2);
d3_std=std(output_d3,0,2);
d_std=[d1_std, d2_std, d3_std];

if ithickness==1
    index=index1;
else
    index=index2;
end

%Averages
d_index_avg=d_avg(index(iangle,ipower),:);
d_output_avg(:,countresults)=d_index_avg';

%Standard Deviations
d_index_std=d_std(index(iangle,ipower),:);
d_output_std(:,countresults)=d_index_std';

countresults = countresults+1;
end
end
end

save('results_discs.mat','d_output_avg','d_output_std')
disp('Done')
%% Output to an excel sheet for later analysis
clear; clc; close all;
load('results_discs.mat')

columns = {'Disc 1' 'Disc 2' 'Disc 3'}';

header = {'Disc #' '0t 0d 0.1W' '0t 0d 0.5W' '0t 0d 1.0W' '0t 45d 0.1W' '0t
45d 0.5W' '0t 45d 1.0W'...
'2t 0d 0.1W' '2t 0d 0.5W' '2t 0d 1.0W' '2t 45d 0.1W' '2t 45d 0.5W' '2t
45d 1.0W'}';

avg_cell = num2cell(d_output_avg);
std_cell = num2cell(d_output_std);

avg = [columns, avg_cell];
std = [columns, std_cell];

avg_output = [header; avg];
std_output = [header; std];

xlswrite('discs_results.xlsx', header,1, 'A1')
xlswrite('discs_results.xlsx', avg_output,1,'A1')

```

```

xlswrite('discs_results.xlsx', header,2, 'A1')
xlswrite('discs_results.xlsx', std_output,2,'A1')

disp('Done')

```

---

## Stacks Results to Excel MATLAB Code

```

%% Code written to export ultrasound-PZT stack data to Excel file
% Written by Morghan Alters.
% Last update: 11/20/19

clear; clc; close all;

load('results.mat')

%% Load Averages and Standard Deviations into an Excel File
% final_results = [resultsavg1, resultsavg2; resultsstd1, resultsstd2];
% excel_results = num2cell(final_results);
%
% labels = {'0.1 W AVG' '0.5 W AVG' '1.0 W AVG' '0.1 W STD' '0.5 W STD' '1.0
W STD'}';
% excel_results = [labels, excel_results];
%
% header = {' ' '0t 0d' '0t 45d' '0t 90d' '2t 0d' '2t 45d' '2t 90d'};
%
% output = [header; excel_results];
%
% xlswrite('excel_results.xlsx', header,1, 'A1')
% xlswrite('excel_results.xlsx', output,1,'A1')
% disp('Done')

%% Load Power vs Resistance Data and St Deviations into an Excel File
rsweep_cell = num2cell(rsweep);

header= {'R' '0t 0d 0.1W' '0t 0d 0.5W' '0t 0d 1.0W' '0t 45d 0.1W' '0t 45d
0.5W' '0t 45d 1.0W'...
        '0t 90d 0.1W' '0t 90d 0.5W' '0t 90d 1.0W' '2t 0d 0.1W' '2t 0d 0.5W' '2t
0d 1.0W'...
        '2t 45d 0.1W' '2t 45d 0.5W' '2t 45d 1.0W' '2t 90d 0.1W' '2t 90d 0.5W' '2t
90d 1.0W'};

all_avgs_cell = num2cell(all_avgs);
all_stds_cell = num2cell(all_stds);

avg = [rsweep_cell, all_avgs_cell];
std = [rsweep_cell, all_stds_cell];

avg_output = [header; avg];
std_output = [header; std];

xlswrite('stacks_results.xlsx', header,1, 'A1')
xlswrite('stacks_results.xlsx', avg_output,1,'A1')

xlswrite('stacks_results.xlsx', header,2, 'A1')
xlswrite('stacks_results.xlsx', std_output,2,'A1')
disp('Done')

```

---

## Individual Disc Results to Excel MATLAB Code

```
%% Main Analysis code written to analyze ultrasound-PZT individual disc data
% and export for later analysis in SAS
% Written by Morghan Alters
% Last update: 12/12/19

clear; clc; close all;

%% Input Parameters

load('input_discs.mat')

max_avg_ind=max_avg_ind-2; %remove the 2 resistances that are omitted in the
single disc sweep
index1=reshape(max_avg_ind(1:9),[3,3]); % rows are power, 1=0.1, 2=0.5, 3=1.0
index2=reshape(max_avg_ind(10:18),[3,3]); % columns are angle, 1=0d, 2=45d,
3=90d

% Removing the 90d trials, and rotating to match subplot layout
index1=index1(:,1:2)'; %rows are now angle of application, 1=0d, 2=45d
index2=index2(:,1:2)'; %columns are now power, 1=0.1, 2=0.5, 3=1.0

frequency = 1e6; % Hz - ultrasound probe frequency

%This is the complete resistance sweep (# of resistors # range of resistors) -
Modify as necessary
resistance_sweep = [0 20 40 60 80 110 140 190 240];

%% Load Desired Data
countresults = 1;

file_path = 'E:\Morghan\TEST\reorganized\';

% Analysis
% Create a FOR loop to analyze CLACS of 0.0mm and 0.8mm
% "i" index , "n" name , "a" abbreviation
for ithickness = 2:2 % Run with 1, then change output names below and to 2
    if ithickness == 1
        nthickness = '0.0mm';
        athickness = '0t';
    else
        nthickness = '0.8mm';
        athickness = '2t';
    end

    %Create a FOR loop to analyze each angle of application
    for iangle = 1:1 % Run from 1:1
        if iangle == 1
            nangle = '0 degrees';
            aangle = '0d';
        else
            nangle = '45 degrees';
            aangle = '45d';
        end

        %Create a FOR loop to analyze each ultrasound power intensity used
```

```

for ipower = 1:3      %Run from 1:3
    if ipower == 1
        npower = '0.1 W';
        apower = '01w';
    elseif ipower == 2
        npower = '0.5 W';
        apower = '05w';
    else
        npower = '1.0 W';
        apower = '1_w';
    end

    %Create a FOR loop to analyze each specimen
    for ispecimen = 1:6      % Run from 1:6
        nspecimen = ['Specimen ' int2str(ispecimen)];

        % Omit the 0.8mm thick, Specimen #3 from our data
        if ithickness==2 && ispecimen==3
            continue
        end

        %Create a For loop to analyze each individual disc
        for idisc = 1:3
            ndisc = ['disc ' int2str(idisc)];
            adisc = ['d' int2str(idisc)];

            for iresistor = 1:length(resistance_sweep)
                % resistance of the oscilloscope
                Rosc=10;

                % Define and read the raw data file
                file_location = [file_path nthickness '\\' nangle '\\'
npower '\\' nspecimen '\\' ndisc '\\'];
                data_file = [athickness '_' aangle '_' apower '_'
int2str(ispecimen) '_' adisc '_' num2str(iresistor), '%.2d.csv'];
                input_name = [file_location data_file];
                data = dlmread(input_name, ',', 2, 0);           % read
in oscilloscope data files

                % Define the output file
                specimen_name = [nthickness ' - ' nangle ' - ' npower
' - ' nspecimen];
                output_file = [file_location specimen_name];

                Rvar = resistance_sweep(iresistor);           % resistance
value in ohms

                % Variable Identification
                time = data(:,1);                               % seconds
                voltage = data(:,2);                             % volts
                voltage = voltage*1000;                          % convert to
mV
                voltage = voltage-mean(voltage);                % center data
around zero

                % Calculate the sample frequency

```

```

                                deltaT = diff(time);                % sampling
freq                                DeltaT = mean(deltaT);          % Side note
may all be the same number          fs = 1 / DeltaT;
between samples                      dt=1/fs;                    % time

                                % Filter
                                fc = 1.2e6;
% cutoff frequency                  [b,a] = butter(5,2*fc/fs);
% (Nth order, cutoff frequency)how to determine cutoff freq
                                Vosc = filtfilt (b,a,voltage);

                                % Variable calculations for voltage and power
                                Vosc = Vosc*(1/sqrt(2));
% convert to RMS voltage            Vout = Vosc.*(1+(Rvar/Rosc));
% scale voltage by the applied resistance - find voltage produced by the
speciman                            Vamp = (max(Vout) - (min(Vout)))/2;
% peak-to-peak voltage (amplitude)  P = Vout.^2./(Rvar+Rosc);
% instantaneous power                Pavg = trapz(time,P) * 1/(max(time) - min(time));
% average power                      Pmax = Vamp.^2./(Rvar+Rosc);
% peak power per cycle                Pmaxu = Pmax*(10^6);
% peak power in uW

                                % Store data to output
                                output(iresistor,1) = Vamp;

                                end

                                if idisc==1
                                    output_d1(:,ispecimen)=output;
                                elseif idisc==2
                                    output_d2(:,ispecimen)=output;
                                else
                                    output_d3(:,ispecimen)=output;
                                end
                                end
                                end

                                all_disc_output = [output_d1, output_d2, output_d3];

                                if ithickness==1
                                    index=index1;
                                else
                                    index=index2;
                                end

                                %Averages
                                d_indexed=all_disc_output(index(iangle,ipower),:);

```



```

        d_output_2t(:,countresults)=d_indexed'; %name as 0t or 2t

        countresults = countresults+1;
    end
end
end

% comment out the line that is not being used above
% save('results_discs_SAS_0t.mat','d_output_0t')
save('results_discs_SAS_2t.mat','d_output_2t')
disp('Done')
%% Output to an excel sheet for later analysis
clear; clc; close all;
load('results_discs_SAS_0t.mat')
load('results_discs_SAS_2t.mat')

results_discs = [d_output_0t, d_output_2t];

columns = {'Disc 1 S1' 'Disc 1 S2' 'Disc 1 S3' 'Disc 1 S4' 'Disc 1 S5' 'Disc
1 S6'...
'Disc 2 S1' 'Disc 2 S2' 'Disc 2 S3' 'Disc 2 S4' 'Disc 2 S5' 'Disc 2
S6'...
'Disc 3 S1' 'Disc 3 S2' 'Disc 3 S3' 'Disc 3 S4' 'Disc 3 S5' 'Disc 3
S6'}';

header = {'Disc #' '0t 0.1W' '0t 0.5W' '0t 1.0W' '2t 0.1W' '2t 0.5W' '2t
1.0W'};

avg_cell = num2cell(results_discs);

avg = [columns, avg_cell];

avg_output = [header; avg];

xlswrite('discs_results_SAS.xlsx', header,1, 'A1')
xlswrite('discs_results_SAS.xlsx', avg_output,1,'A1')

disp('Done')

```

---

## Statistical Analysis SAS Code

```

/* PZT-Ultrasound statistics analysis on stacks data
Written by Morghan Alters
Modified from code written by Craig Cunningham
Last updated: 11/25/19 */

/* Clears the log */
dm 'log;clear';
/* Clears the output */
dm 'output;clear;';

/* Change the data file for each statistical analysis (21 different ones used) */
proc import datafile='/folders/myfolders/1-Effect of Intensity/SAS-1.csv'
out=work.stacks
dbms=CSV
REPLACE
;
run;

```

```

/*=====
checking assumptions/requirements (START)
=====*/
*running 1-way model;
*this will allow a Normality test/plots, as well as an HOV plot (no test);
PROC GLM DATA=stacks;
CLASS group ;
MODEL power = group;
MEANS group ;
OUTPUT OUT=junk PREDICTED=yhat RESIDUAL=e;
QUIT;
PROC UNIVARIATE DATA=junk NORMAL PLOT;
VAR e;
RUN;
/*Plot the residuals vs predicted-y value to assess the homogeneity of variance assumption*/
PROC SGPLOT DATA=junk;
SCATTER Y=e X=yhat;
RUN;
/*Transforms the dependent variable in order to achieve the normality of residuals and homogeneity of
variance assumptions */
DATA stacks;
SET stacks;
power_log = log(power);
RUN;
/*Re-run the PROC GLM section and check for equal variance and normality with the transformed variables*/
PROC GLM DATA=stacks;
CLASS group ;
MODEL power_log = group ;
OUTPUT OUT=junk PREDICTED=yhat RESIDUAL=e;
QUIT;
PROC UNIVARIATE DATA=junk NORMAL PLOT;
VAR e;
RUN;
PROC SGPLOT DATA=junk;
SCATTER Y=e X=yhat;
RUN;
/*=====
checking assumptions/requirements (END)
=====*/
*this is the main code that analyzes where the significant results occur
*tukey-kramer post-hoc

PROC GLM DATA=stacks;
CLASS group ;
MODEL power_log = group;
OUTPUT OUT=junk PREDICTED=yhat RESIDUAL=e;
LSMEANS group / CL LINES PDIF=ALL ADJUST=TUKEY ALPHA=0.05;
QUIT;

```